Title: Piezo1 and Piezo2 channels in retinal ganglion cells and the impact of Piezo1 stimulation on light-dependent neural activity

Authors: Puttipong Sripinun[1,2,7], Lily P. See[1,3], Sergei Nikonov[4], Venkata Ramana Murthy Chavali[5], Vrathasha Vrathasha[5], Jie He[5], Joan M. O'Brien[5], Jingsheng Xia[1], Wennan Lu[1], Claire H. Mitchell[1,6*]

Author Affiliation:
Departments of Basic and Translational Science[1], Orthodontics[2], Endodontics[3], Neuroscience[4], Ophthalmology[5], Physiology[6], University of Pennsylvania, Philadelphia, PA 19104. Department of Orthodontics and Pediatric Dentistry, Chiang Mai University, Chiang Mai, Thailand, 50200[7].

Corresponding Author: Dr. Claire H. Mitchell, Department of Basic and Translational Science, University of Pennsylvania, 440 Levy Building, 240 S. 40th St, Philadelphia, PA 19104, Tel. 215 573-2176. E-mail: chm@upenn.edu

Key words: Piezo, ion channel, mechanosensitive, retinal ganglion cells, RGC excitability, neuron, axons, glaucoma

Word count (main text)**:** 6,787

Abstract

Piezo channels are associated with neuropathology in diseases like traumatic brain injury and glaucoma, but pathways linking tissue stretch to aberrant neural signaling remain unclear. The present study demonstrates that Piezo1 activation increases action potential frequency in response to light and the spontaneous dark signal from mouse retinal explants. Piezo1 stimulation was sufficient to increase cytoplasmic Ca^{2+} in soma and neurites, while stretch increased spiking activity in current clamp recordings from of isolated retinal ganglion cells (RGCs). Axon-marker beta-tubulin III colocalized with both Piezo1 and Piezo2 protein in the mouse optic nerve head, while RGC nuclear marker BRN3A colocalized with Piezo channels in the soma. Piezo1 was also present on GFAP-positive regions in the optic nerve head and colocalized with glutamine synthetase in the nerve fiber layer, suggesting expression in optic nerve head astrocytes and Müller glia end feet, respectively. Human RGCs from induced pluripotent stem cells also expressed Piezo1 and Piezo2 in soma and axons, while staining patterns in rats resembled those in mice. mRNA message for *Piezo1* was greatest in the RPE/choroid tissue, while *Piezo2* levels were highest in the optic nerve, with both channels also expressed in the retina. Increased expression of *Piezo1* and *Piezo2* occurred both 1 and 10 days after a single stretch *in vivo;* this increase suggests a potential role in rising sensitivity to repeated nerve stretch. In summary, Piezo1 and Piezo2 were detected in the soma and axons of RGCs, and stimulation affected the light-dependent output of RGCs. The rise in RGCs excitability induced by Piezo stimulation may have parallels to the early disease progression in models of glaucoma and other retinal degenerations.

Highlights

- Activation of Piezo1 excites retinal ganglion cells, paralleling the early neurodegenerative progression in glaucoma mouse models and retinal degeneration.
- Piezo1 and Piezo2 were expressed in axons and soma of retinal ganglion cells in mice, rats, and human iPSC-RGCs.
- Functional assays confirmed Piezo1 in soma and neurites of neurons.
- Sustained elevation of *Piezo1* and *Piezo2* occurred after a single transient stretch may enhance damage from repeated traumatic nerve injury.

Introduction

Throughout the body, mechanical stimuli are converted into electrochemical signals through the process of mechanotransduction. Excessive mechanical strain on nervous tissue, whether acute or chronic, can manifest as inflammatory events, loss of neural function, and, in some cases, death of the neuron [1,2]. Linking mechanical strain to these responses is thus critical in understanding the signaling pathways that contribute to their pathogenesis [3,4].

Piezo ion channels are pore-forming mechanosensitive cation channels [5,6]. They are uncommonly large, consisting of over 2100 amino acids and 24- 36 transmembrane regions; the extensive surface area of the channel facilitates the sensing and transduction of mechanical stimuli into downstream signaling events [7,8]. The Piezo channels are permeable to cations, where membrane stretch gates the pore opening, leading to influx of Na^+ and Ca^{2+}, among others, causing membrane depolarization under physiological gradients [9,10]. There are two Piezo isoforms: Piezo1 was traditionally associated with non-neuronal tissues, and Piezo2 with sensory neurons [8]. However, synergistic interactions and interdependence between the isoforms suggest these divisions are not binary [5,11]. In addition to being mechanosensitive themselves, Piezo channels can mediate the downstream modulation of other mechanosensitive ion channels,

making them primary regulators of cellular mechanosensitivity [12,13]. The contributions of Piezo channels to mechanotransduction in neural tissues under baseline and stressed conditions remain unclear, with increasing evidence suggesting possible roles of not only Piezo2 but also Piezo1 in neurons [14-17].

Retinal ganglion cells (RGCs) are particularly vulnerable to mechanical strain as their path from soma to synapse in the brain requires the unmyelinated axon to transverse the optic nerve head region as they exit the ocular chamber. The mechanical forces driven by the pressure gradients between the cerebrospinal fluid pressure and intraocular pressures (IOP) are greatest here and are exacerbated when IOP rises in glaucoma [18,19]. Increased forces across the optic nerve head region remain a primary risk factor for neural degeneration and death of RGCs in glaucoma [20-23]. While several studies have investigated the presence of Piezo channels in the retinal and optic nerve regions, considerable discrepancies remain [24-27]. The use of a single species and limited approaches likely added to the confusion. A more rigorous examination of Piezo channels in the neurons and glia of the optic nerve head region is needed, particularly given a recent investigation implicating Piezo1 mutations in some forms of glaucoma [28].

The present study uses molecular tools, immunohistochemistry, microelectrode array, and live cell Ca^{2+} imaging to examine the expression of Piezo1 and Piezo2 in the retinal tissue of mice, rats, and human RGCs derived from induced pluripotent stem cells (iPSC-RGCs). Of particular interest is the presence of both Piezo1 and Piezo2 in the axons of RGCs, the response in live RGCs to Piezo1 agonist Yoda1, the rise in *Piezo1* and *Piezo2* expression 10 days after a transient stretch, and increase in the excitability of the RGCs in explant retinal tissue. These findings support the neural expression of both Piezo1 and Piezo2 and suggest that a single stretch can prime neural tissues, increasing their sensitivity for future responses and may potentially alter the visual perception in patients.

Methods

Animal Care and Use: Animal experiments were performed in strict accordance with the National Research Council's "Guide for the Care and Use of Laboratory Animals" and were approved by the University of Pennsylvania Institutional Animal Care and Use Committee (IACUC) protocol #803584. All animals were housed in temperature-controlled rooms under 12:12 light–dark cycles with food and water ad libitum. Long–Evans rats of 12 months (Harlan Laboratories/Envigo, Frederick, MD, United States), and C57BL/6J mice of 3-6 months (Jackson Laboratories, Bar Harbor, ME, United States) of both sexes were utilized.

iPSC-RGC culture: iPSC-RGC development and growth was performed as described previously with minor modifications [29]. Human iPSCs were kept on dishes coated with 1:100 diluted growth factor reduced Matrigel (Corning) and maintained in iPSC medium (StemMACs iPS-brew XF, Human, Miltenyi Biotec) with the addition of 20 ng/mL bFGF. Once cells attained 75% confluence; 5 ng/mL stable bFGF was added. iPSCs were kept at 37 °C with 5% O_2 and 5% CO_2 until 100% confluent, then transferred overnight to 5% CO_2 to initiate RPC/RGC induction. On day 0, media was changed to RPC induction media: DMEM/F12 (50:50), 1% P/S, 1% Glut, 1% NEAA, 0.1 mM 2-ME, 2% B27 supplement (w/o vitamin A), 1% N2 supplement. Daily additions of fresh media including 2 μM XAV939, 10 μM SB431542, 100 nM LDN193189, 10 mM nicotinamide, and 10ng/mL IGF1 were performed. Nicotinamide was replaced with 10ng/ml bFGF on days 4-21. RGC induction media was introduced on day 22, composed of DMEM/F12: Neurobasal media, 1:1, 1% P/S, 1% Glut, and 2% B27. In addition, 250ng/ml SHH, 100ng/ml FGF8 and 3uM DAPT were added to media on days 22-23. On day 24, cells were cross-hatched and passaged onto Matrigel coated plates for RGC differentiation with 3μM DAPT, and 100ng/ml Follistatin included in the RGC medium. Cyclopamine 0.5μM was included on day 24 only. RGC maturation was induced on days 27-35 with addition of 3μM DAPT, 10μM Y27632, 400μM cAMP, 5μM forskolin, 40ng/ml BDNF, 5ng/ml NT4 and 10ng/ml CNTF. Cell media was changed daily from days 0-26,

and every 3 days from days 27-35. After day 36, RGCs were maintained in RGC induction media with DAPT and Y27632 with media changed 2x/ week. The iPSC-RGCs produced were shown to express markers RPBMS and BRN3A and produce action potentials when depolarized [29], supporting their identity as RGCs.

RGCs in mixed retinal cell culture: RGCs were cultured in mixed retinal cultures as these cells are healthier than those grown under isolated conditions [30]. To ease the identification of RGCs, cultures were generated from P3-10 *Slc17a6*$^{Cre+}$; *R26R*$^{tdTomato+}$ mouse pups. tdTomato-labeled RGCs mice (*Slc17a6*$^{Cre+}$; *R26R*$^{tdTomato+}$), *Slc17a6*-driven Cre (*Slc17a6*$^{Cre+/+}$; strain number 028863) mice were mated with Ai9 mice (*R26R*^{tdTomato}; strain number 007909*)*, which express CAG promoter-driven tdTomato expression upon Cre-mediated recombination, thereby removing loxP-flanked STOP cassette allowing for a transcription of red fluorescent tdTomato as described [31]. Tail DNA was used for genotyping confirmation and analyzed using the primer sequences and PCR protocols following manufacturer guidelines (Jackson Laboratories). To generate mixed retinal cultures, pups from both sexes were euthanized and retinas were promptly dissected in HBSS (Cat# 14175079; Gibco). Retinas were then incubated in digestion media containing papain (16.5U/mL; Cat# LK003176; Worthington) and DNase I (12,500U/mL; Cat# LK003170; Worthington) for 30 mins at 37°C followed by trituration in RGC culture media and centrifugation. Cells were then plated on poly-D-lysine and mouse laminin I-coated 12 mm Nunc glass base dish (Cat# 150680; Thermo Scientific) and cultured for 3-5 days in the RGC culture medium prior to the calcium imaging experiment. RGC culture media was based on the enriched serum-free growth media as described [32]; RGC growth and survival were substantially improved as compared to approaches used previously in the laboratory [33]. The media containing a 1:1 mix of base media of DMEM (Cat# 11960044; Gibco) and neurobasal (Cat# 21103049; Gibco), insulin (5 µ g/mL; Cat# I6634; Sigma), sodium pyruvate (1mM; Cat# 11360-070; Sigma), NS21 supplement (Cat# AR008; R&D systems), penicillin/streptomycin (1%, Cat # 15140-12; Gibco), SATO supplement

(1X; in house-made) [34], L-glutamine (2mM, Cat# 25030-081; Gibco), triiodothyronine (T3, 40 ng/ml, Cat# T6397; Sigma), brain-derived neurotrophic factor (BDNF; 50 ng/mL; Cat# 450–02; Peprotech, Rocky Hill, NJ), ciliary neurotrophic factor (CNTF; 10 ng/mL; Cat# 450–13; Peprotech), and forskolin (4.2ng/mL; Cat# F6886; Sigma Aldrich). Half of the growth medium was changed every 2–3 days.

Culture of optic nerve head astrocytes: Primary mouse optic nerve head astrocyte cultures were dissected from neonatal mice (PD1-7) of both genders based on a protocol modified from Albalawi et al. [35]. In brief, optic nerve head tissue was digested in 0.25% trypsin (Invitrogen, Carlsbad, CA) for 30 mins at 37°C, followed by light trituration in culture media; this loosens up the optic nerve tissue to facilitate astrocyte outgrowth. The material was re-suspended in growth media containing DMEM, 10% FBS, 1% penicillin/streptomycin, and 25 ng/mL murine epidermal growth factor (#E4127, Sigma–Aldrich) and plated on 35 mm culture dishes pre-coated with poly-D-lysine and grown at 37°C, 5% CO_2. Dishes usually approached confluence within 10 days. Astrocytes were generally used at passage 4 or below.

Microelectrode array (MEA) recordings: MEA recordings were performed following previously described methods [36,37] on C57BL/6J mice dark-adapted for at least 2 hours. Dorsal retinal patches were positioned with the ganglion cell layer facing downward on the square array of 60 electrodes (200 µm interelectrode distance) in the MEA recording chamber (60MEA200/30iR-Ti-gr; Multi Channel Systems) mounted on the 1060i amplifier (Multi Channel Systems, Reutlingen, Germany). Gentle suction was carefully applied to generate negative pressure bellow the sample, improving electrode-to-tissue contact and the signal-to-noise ratio. During the recording, perfusion of oxygenated Ames' solution (#A1420, Sigma–Aldrich) at 37°C was continuously supplied to the chamber to support the physiological health condition of the retinal tissue. The Piezo1 agonist Yoda1 was added to the perfusate as indicated. Retinal stimulation included series of ten 2-second flashes of 455 nm light (~60% efficiency in driving mouse rhodopsin compared to

500 nm light) delivered at 0.1 Hz. All flashes in a series had the same intensity, three different intensities in the scotopic range (32, 117, and 377 hv s^{-1} μm^{-2}) were used for the stimulation. Data capture was acquired by an NI PCI-6071E DAQ board and custom software developed in LabView (National Instruments, Austin, TX, USA), and later analyzed using MATLAB-based custom coding (MATLAB, Natick, MA, USA).

Ca^{2+} measurement from RGCs and optic nerve head astrocytes: To determine the physiologic responses from axons and somas, levels of Ca^{2+} in RGCs were determined microscopically, based on approaches described in detail previously [38]. In brief, mixed retinal cultures were loaded with 5 μM Fura-2 AM (acetoxymethyl ester, #F1221; Thermo Fisher Scientific) with 0.01% pluronic F-127 (#P3000MP; Thermo Fisher Scientific) at 37°C for 45 min. Cells were washed, mounted in a perfusion chamber, and visualized using a ×40 objective on a Nikon Diaphot microscope (Nikon, Melville, NY, USA). Ratiometric measurements were performed by alternating the excitation wavelength from 340 to 380 nm and quantifying emission ≥512 nm with a charge-coupled device camera (All Photon Technologies International, Lawrenceville, NJ, USA); the tdTomato assisted in identifying the RGCs but did not interfere with the Fura-2 signal. Cells were perfused with isotonic solution containing 105 mM NaCl, 5 mM KCl, 6 mM 4-(2-hydroxyethyl)-1-piperazineethanesulfonic acid, 4 mM Na 4-(2-hydroxyethyl)-1-piperazineethanesulfonic acid, 5 mM $NaHCO_3$, 60 mM mannitol, 5 mM glucose, and 1.3 mM $CaCl_2$; the Piezo1 agonist Yoda1 (Cat# SML1558, Sigma) and gadolinium (Cat# 01128606, Thermo Fisher) was added to the perfusate for the time indicated.

Given the homogeneity of optic nerve head astrocytes grown in isolation, Ca^{2+} was measured using a plate reader. Astrocytes were grown to confluence in 96-well black assay plates with clear bottoms for 4 –7 days (Cat# 353219; Corning) and loaded with Fura-2 AM and 0.02% Pluronic F-127 in culture media for 45 min at 37°C, followed by a 30 min period for de-esterification. Cells were washed and placed in isotonic solution, and changes in cytoplasmic Ca^{2+}

levels were determined from the ratio of light excited at 340 and 380 nm (510 nm emission) using a Varioskan™ LUX multimode microplate reader (Thermo Fisher). Yoda1 was introduced using the internal injector system and was not washed off.

Retinal stretch with IOP elevation in mice: The IOP was elevated in mice using a modified version of the Control Elevation of IOP (CEI) protocol developed by Morrison et al. [39] and used previously [40,41]. This procedure separates the acute effects of increased IOP from cell death to focus more on the consequences of mechanical strain. In brief, C57BL/6J mice ages 3-6 months were anesthetized and maintained with 1.5% isoflurane throughout the procedure after receiving 5 mg/kg meloxicam. Corneal anesthesia and mydriasis were achieved by administering proparacaine (0.5%) and tropicamide (1%) eye drops, respectively. One eye was cannulated with a 33-gauge needle attached to polyethylene tubing (PE 50; Becton 51 Dickinson) inserted into the anterior chamber, connected to a 20 ml syringe filled with sterile Hank's Balance Salt Solution. IOP was elevated to 58 mmHg by positioning the reservoir to the appropriate height; this pressure was selected to maintain retinal blood flow and avoid ischemia [42-44] Ocular lubricant gel was applied at regular intervals to both eyes to prevent corneal desiccation (GenTeal; Alcon laboratory, Fort Worth, TX). The needle was removed after 4 h and IOP returned to baseline, with 0.5% erythromycin ointment applied to the cornea. The contralateral eye served as a normotensive control. Mice were euthanized 1 or 10 days later. A sham control mice were also conducted where needle insertion without elevation of intraocular pressure was performed in a similar manner as the experimental group.

PCR and Real-Time qPCR: Murine eyes were enucleated and promptly dissected in HBSS. The anterior portion of the eye was removed, followed by the iris and lens. Three tissues were collected at this stage under the dissecting microscope: the neuronal retina was detached from the eyecup, RPE sheets were gently peeled off from the underlying Bruch's membrane by using a microsurgical Iris Spatulae, and optic nerve starting from the proximal portion of the sclera. All

tissues were stored in TRIzol reagent (Invitrogen) at -80 ºC until further processing for RNA. Total RNA was extracted with PureLink™ RNA Mini Kit (Invitrogen) and RNeasy Micro Kit (Qiagen). cDNA was synthesized from 250 and 500 ng of total RNA per reaction using the High Capacity cDNA Reverse Transcription Kit (Applied Biosystems, Waltham, MA) for PCR and RT-PCR experiments, respectively, as described [40,45]. PCR amplification of cDNA was performed using AmpliTaq Gold DNA Polymerases with Gold buffer and $MgCl_2$ (Thermo Fisher, Carlsbad, CA) following the manufacturer's instructions. The PCR products were then run on 2% agarose gels and visualized by ethidium bromide staining, along with a 100-bp DNA ladder (Thermo Fisher, Carlsbad, CA). The real-time quantitative polymerase chain reaction (Real-Time qPCR) was performed using SYBR Green and the 7300 RealTimePCR system (Applied Biosystems). All data were analyzed using the delta-delta Ct approach. *Gapdh* was utilized as an endogenous control. The primer sequences and expected product sizes are given in Table 1.

Immunohistochemistry: Animals were perfused intracardially, and dissected eyes were postfixed with 4% paraformaldehyde. Piezo channels were identified by immunohistochemical staining in 10 µm sections from rodent retina and human iPSC-RGCs. Sections and cells were fixed with 4% paraformaldehyde for 10 minutes, permeabilized with 0.1% Triton X-100 (Sigma-Aldrich) and 20% SuperBlock buffer (ThermoFisher) in 0.1% PBS-T for 10 minutes at 25 °C, then blocked with 10% donkey serum and 20% SuperBlock in PBS-T for 1 hour, followed by primary antibodies overnight at 4°C, and by secondary antibodies for 1 hour at 25 °C. The list of antibodies is provided in Table 2. Autofluorescence quenching was performed on retinal tissues using the TrueVIEW Autofluorescence Quenching Kit (Vector Laboratories, Burlingame, CA) as outlined by the manufacturer. After incubation with DAPI (Sigma-Aldrich) for 10 min, slides were washed and mounted using SlowFade Gold (Thermo Fisher). Imaging was performed using a Nikon E600 epifluorescence and Eclipse confocal Ti2- microscope with NIS Elements Imaging software (Nikon v. 4.60).

Data analysis: Statistical analysis was performed using GraphPad Prism software version 10 (GraphPad Software, LLC). Bars represent mean ± standard deviation, with individual data points from each retina, sample, or image depicted as dots, as appropriate. Significant differences between two unrelated groups were assessed by unpaired t-test; paired Student's t-tests were employed when comparing the eyes of the same mouse. One-way ANOVA followed by Tukey's tests was used to compare three or more means. Statistical significance showed at p-value > 0.05 = ns, * p-value < 0.05, ** p-value < 0.01, *** p-value < 0.001, and ****p < 0.0001.

Results

Piezo1 and Piezo2 messages are expressed in mouse retina, RPE/Choroid, and optic nerve and sustainably upregulated with a transient elevation of IOP in vivo.

To provide an overview of Piezo message levels in the adult mouse, initial experiments examined the relative expression of mRNA for *Piezo1* and *Piezo2* in regions of the posterior mouse eye. Traditional PCR demonstrated the presence of *Piezo1* mRNA in the retina, RPE-choroid, and optic nerve regions of C57BL/6 mice. Bands were of the expected size of 176 base pairs, with the most intense band from the RPE-choroid tissue. PCR also showed that *Piezo2* was expressed in the retina, RPE-choroid, and optic nerve regions, with the predicted size of 222 base pairs; expression was greatest in material from the optic nerve and RPE-choroid (Fig. 1A).

To further analyze the expression of *Piezo1* and *Piezo2* messages in the posterior eye, we utilized real-time semi-quantitative PCR (qPCR). The relative expression of *Piezo1* mRNA was greatest in material from the RPE-choroid, with levels 30-fold greater than in the retina. Levels of *Piezo1* expression were 5-fold greater in the optic nerve than in the retina. *Piezo2* gene expression was highest in the optic nerve, with expression >200-fold higher than in the retina, while expression of *Piezo2* was 160-fold higher in the RPE-choroid than in the retina (Fig. 1B). The convergence between results from traditional PCR and qPCR regarding the relative

expression of Piezo message strongly supports the finding that *Piezo1* and *Piezo2* are expressed in all three types of tissues, with the greatest expression in RPE choroid and optic nerve tissue, respectively, when compared to the neural retina.

Stretch is recognized as a key force impacting optic nerve head and retinal tissue following the elevation of IOP [46,47]. To determine whether a single exposure to stretch altered the expression of Piezo channels, a modified version of the Controlled Elevation of IOP (CEI) procedure was used to examine the timescale of Piezo channel upregulation; the CEI procedure can induce RGC damage following a single interval of pressure elevation that resembles that found with more chronic rises [39]. Mice were sacrificed 1 day or 10 days after a 4-hour hypertensive episode, as a recent investigation suggests inflammatory signals can remain elevated 10 days after a single elevation of IOP [48].

A significant upregulation in the expression of both *Piezo1* and *Piezo2* was found in mouse retina stretched with the CEI procedure. *Piezo1* and *Piezo2* expression levels increased 1.7-fold and 2-fold, respectively, 1 day after the return to baseline IOP levels (Fig.1C). Both Piezo isoforms remained significantly elevated 10 days after the event (Fig. 1D). Sham control with the needle inserted in a similar fashion as the experimental group while no elevation of intraocular pressure was used as control where no significant changes can be seen (Fig. 1E). Together, these findings suggest an increase in *Piezo* expressions after a single IOP elevation that could prime the retina, producing increased responses to subsequent increases in pressure.

Electrophysiological study using ex vivo retinal MEA recording revealed enhanced RGC excitability via Piezo1 activation.

Specific agonists that can selectively activate Piezo channels are of great interest and are crucial for examining the roles of Piezo channels in physiological and pathological processes. However, currently, only Piezo1-specific agonists have been identified, while Piezo2 remains an area of ongoing research. To determine the effect of Piezo1 ion channel activation on RGC

physiological function, a specific Piezo1 agonist, Yoda1 was used in an established MEA experiment to assess any alteration in spike firing of RGCs from retinal explants. During the course of the experiment, continuous spontaneous firing was notably observable during periods of rest, while substantial activity in the firing of RGCs was elicited at the commencement and conclusion of the light stimulus. With the perfusion of Yoda1 to the system, mean spontaneous firing rates of RGCs significantly increased by 41.16% from the control. This phenomenon continued as Yoda1 remains in the perfusion (Fig. 2A,B) and can be partially alleviated by removing Yoda1 from the system (Fig. 2B).

To further examine the effect of Piezo1 activation on the scotopic condition, a series of ten 2-second flashes at different intensities were used to evoke ON- and OFF-RGC firing activities (Fig. 2C). Analysis revealed a modest but significant increase in light-evoked ON and OFF RGC transient firings (Fig. 2D,E). These findings support the evidence of Piezo1 channel expression in the retina, and its activation can heighten the excitability of RGCs, suggesting high mechanosensitivity within these neuronal cells mediated through Piezo1 channel. Further support comes from patch clamp trials indicating that RGCs display pressure-sensitive currents and increase spiking activity when pressure is applied through a high-speed pressure clamp (Fig. S1, S2). This is consistent with the increased spiking activity found with Yoda1.

Physiological confirmation of Piezo1 in RGCs and optic nerve head astrocytes

A functional confirmation of Piezo1 in RGCs was determined utilizing Yoda1, a specific activator of Piezo1, with an EC_{50} at mouse Piezo1 of 17.1 μM and no reported activation of Piezo2 at levels under 100 μM [49]. Measurements were obtained from RGCs in mixed retinal cultures from *Slc17a6*$^{Cre+}$; *R26R*$^{tdTomato+}$ mice to aid in identifying RGC soma and neurites; inspection indicated extensive growth of neurites (Fig. 3; A1). RGCs were loaded with the Ca^{2+} indicator Fura-2 as the low excitation wavelengths of 340 and 380 nm did not interfere with the tdTomato signal, while the ratiometric signal was more reliable than single wavelength reporters. Microscopic examination enabled measurement from soma and neurites. Application of 50 μM Yoda1 led to a

rapid rise in intracellular Ca^{2+} (Fig. 3; A2). The response was reversible, with levels returning to baseline before Yoda1 was removed. The rise in cytoplasmic calcium observed in both soma and neurites of the RGCs was similar, with no significant difference in magnitude between them (Fig. 3; A3). In addition, a broad-spectrum mechanosensitive cation antagonist, gadolinium (Gd^{3+}), was able to inhibit yoda1-induced intracellular calcium elevation (Fig. 3; A4,5).

Further validation of the response to Piezo1 stimulation was examined in mouse optic nerve head astrocytes. The astrocytes stained clearly for both GFAP and Piezo1 (Fig. 3; B1). Staining for Piezo1 was particularly evident on the astrocyte extensions. A similar staining was found for Piezo2 (not shown). Stimulation of the astrocytes with Yoda1 induced a dose-dependent elevation of intracellular Ca^{2+} (Fig. 3; B2,3). The rise in Ca^{2+} induced by Yoda1 in the astrocytes was sustained in the continued presence of Yoda1.

Detection in RPE cells and validation of antibody specificity

Upon identifying transcripts and functionality of Piezo channels in the retina and considering their potential role in modifying the function of RGCs, we proceeded to investigate the spatial distribution of Piezo channels within the retinal tissues using immunohistochemistry. Although antibodies developed in the past few years have shown improved specificity for Piezo1 and Piezo2 with several genetic modification tool evaluations to support the claims [50-57], validation is always needed, so the specificity of the Piezo antibodies used in this study was confirmed. The human retinal pigment epithelial cell line (ARPE-19) was treated with *Piezo1*-targeted siRNA for 48 hours; *Piezo1* siRNAs reduced Piezo1 expression by > 85%. Robust staining for Piezo1 was detected in RPE cells under control conditions but reduced with *Piezo1*-targeted siRNA (Fig. S3B). Quantification of fluorescent intensity confirmed a significant reduction (Fig. S3C). Similar results were found with siRNA targeting *Piezo2*, with a 77% reduction in message (Figure S3D) and decline in immunostaining (Fig. S3E,F). These observations suggest the antibodies used in this study show reasonable specificity, in agreement with previous confirmation reported [50-57],

while also confirming the detection of message for both *Piezo1* and *Piezo2* in the RPE/choroid tissue above.

Immunohistochemical identification of Piezo1 in mouse neural retina and optic nerve

The validated antibody was used to examine Piezo1 expression in the adult C57BL/6 mouse retina. Staining for Piezo1 was evident in the nerve fiber layer and cell bodies located in the ganglion cell layer (Fig 4A). Overlap between staining for Piezo1 and glutamine synthase was observed along the internal limiting membrane at the nerve fiber layer (Fig. 4A), suggesting the presence of Piezo1 on the end feet of Müller cells [58]. Further investigation was proceeded to rule out cell types with positive staining of Piezo1 in the ganglion cell layer.

The neuronal microtubule marker, beta-tubulin III, was used to identify RGCs [59,60]. Positive co-staining between beta-tubulin III and Piezo1 was observed around the RGC cell bodies, though lesser degree of Piezo1 was found in RGC dendrites and axons (Fig. 4B). Close association between Piezo1 and RGC nuclear marker BRN3A [61] also suggested expression of Piezo1 in RGC cell bodies (Fig. 4C). Similar immunolabeling was also performed with another validated antibody by other studies where staining in RGC cell bodies can also be seen, supports the premise of Piezo1 expression in RGCs (Fig. S5).

The optic nerve head also displayed staining for both Piezo1 and beta-tubulin III, with colocalization along the nerve bundles in a heterogeneous punctate pattern. Interestingly, Piezo1 demonstrated a banding staining pattern perpendicular to the nerve evident at the lamina cribrosa (white arrow), where astrocytes are situated (Fig. 4D). Glial fibrillary acidic protein (GFAP) staining was then used to identify astrocyte [62] together with Piezo1 at the optic nerve head, where overlapping of both antigens were evident along the glial laminar (Fig. 4E).

Immunohistochemical identification of Piezo2 in neural retina and optic nerve head of mouse

The expression and distribution of Piezo2 was also examined in the mouse. Piezo2 displayed prominent staining in the nerve fiber layer, showing strong colocalization with beta-

tubulin III (Fig. 5A). Piezo2 and beta-tubulin III co-staining continued through the optic nerve head region and into the optic nerve, with the striated staining suggesting localization within the axons. Staining was also detected in RGC soma, with some cells also displaying Piezo2 in beta-tubulin III-positive dendrites. Piezo2-stained cells were found to surround BRN3A positive nuclei (Fig. 5B), confirming Piezo2 expression in RGCs. Minimal staining for Piezo2 was observed in the outer retina.

Piezo1 and Piezo2 expression in human iPSC-RGCs

To further characterize the expression of Piezo channels and increase the relevance to humans, we examined human induced pluripotent stem cell-derived retinal ganglion cells (iPSC-RGCs). Cells derived using this process are electrically active and express key RGC markers [29,63]. Identification was confirmed with iPSC-RGCs staining for markers BRN3A and RBPMS (Fig. 6A). Particulate staining for Piezo1 was detected in the soma and neurites of iPSC-RGCs (Fig. 6B); staining for Piezo2 was similar but more robust. Strong co-localization between Piezo2 and beta-tubulin III was evident, particularly in the neurites (Fig. 6C).

Immunohistochemical identification of Piezo1 and Piezo2 in neural retina and optic nerve of rat

Immunolocalized experiments were repeated in the rat retina to support the identification in mouse and human material. Staining of Piezo1 in rat retina was similar to that in the mouse, although with more intense staining observed along the internal limiting membrane (Fig. 7A). Colocalization with beta-tubulin III supported Piezo1 in some RGC soma. Light particulate immunoreactivity of Piezo1 between strands of beta-tubulin III-positive regions was noticed throughout the optic nerve head. Piezo2 staining was also similar in rat to that observed in mouse, with clear colocalization in the nerve fiber layer and weaker staining in the soma and dendrites of RGCs (Fig. 7B). Staining for Piezo2 and beta-tubulin III was also present throughout the optic nerve head of rat tissue.

Discussion

The present study provides an analysis of Piezo channels in the retina, using multiple approaches and models to strengthen conclusions. The presence of both Piezo1 and Piezo2 channels was particularly robust in RGCs. The co-localization between beta-tubulin III and Piezo1 suggests channel expression in somas and axons of nerve fibers. The staining of iPSC-RGCs showed a similar pattern, while Yoda1 increased Ca^{2+} in the soma and neurites of cultured mouse RGCs. Robust staining of Piezo 2 was detected in mouse, rat and human RGCs, with particularly strong staining in the axons of the nerve fiber layer and through the optic nerve head. Staining for Piezo1 was also colocalized with markers for astrocytes in the optic nerve head and Müller cells at their end feet. Together, the results implicate Piezo1 and 2 channels in homeostatic processes of adult RGC axons, with contributions suggested from Müller cells and optic nerve head astrocytes.

Analysis of mRNA levels also suggests expression of both *Piezo1* and *Piezo2* in the retina, optic nerve, and the RPE/choroid. While expression of both channels was relatively low in the retina, this likely reflects the presence of the channels in only a few of the retinal cell types. The robust expression of message for *Piezo1* and *Piezo2* in the RPE/choroid was unexpected, given the tissues are non-excitable and not traditionally thought of as mechanosensitive. While immunostaining for both Piezo1 and Piezo2 in ARPE-19 cells supports this identification, confirmation in vivo is currently being investigated.

Dysfunction in neuronal signaling pathways, including RGC function, has been associated with alterations in IOP dynamics [64]. Early compensatory response in RGCs characterized by increased excitability levels in both ON and OFF subtypes, irrespective of the extent of dendritic pruning, have been identified as a notable feature of the initial stages of neurodegeneration in glaucoma models. Risner et al. observed that following two weeks of microbead-induced IOP elevations in mice, representing an early time-point in disease propagation, there was a noticeable increase in depolarization of the resting membrane potential of RGCs, leading to a

lowered excitation threshold. Furthermore, responses to the onset of light stimuli also exhibited increased magnitude, duration, and frequency. However, these enhancements were transient and undetectable at four weeks of sustained IOP elevation [65]. Tao et al. demonstrated that alterations in RGC function, including an increase in spontaneous firing rate and excitability, were evident only under conditions of microbead-induced IOP elevation at lower magnitudes but not at higher IOP levels [66]. Strikingly, our findings suggested that Piezo1 may play a role in this early adaptive role in glaucoma as the results emulate what had been described previously *in vivo*, where RGCs modify their physiology to maintain functionality, mitigating affected RGCs to improve signaling between neurons.

The presence of both Piezo1 and Piezo2 in RGC stresses the importance of mechanosensitivity to these neurons. While the two Piezo isoforms are often expressed in different cell types, evidence for the expression of both isoforms is emerging [11,67-69]. Simultaneous labeling for Piezo1 and Piezo2 was hampered by a shared host for reliable antibodies, but the expression of both channels in most RGC axons supports co-expression in at least some cells. The co-expression of message for both Piezo1 and 2 was recently described in cells of the anterior eye [27]. The expression of both Piezo1 and 2 in these neurons is of interest given that they can show synergistic actions [67] and may compensate for changes in one another's expression [11]. It remains to be determined whether a similar interaction occurs between Piezo1 and Piezo2 in RGC axons. However, the robust expression of both channels in the axons may reflect the importance of the contribution of Piezo channels to the neurons.

Strengths of the study and comparison to others

Confidence in the findings of the current study is enhanced by several aspects of the experimental design. The molecular and protein data converge, with expression of mRNA found with PCR and qPCR (Fig. 1) in agreement with that found on the protein level with immunohistochemistry (Fig. 4-7). The agreement between expression patterns in the mouse (Fig.

4-5) and rat (Fig. 7) retina, and in human iPSC-RGCs (Fig. 6) also supports the conclusions. The ability of Yoda1 to induce Ca^{2+} influx into RGCs adds a functional confirmation of Piezo1 in RGCs and optic nerve head astrocytes (Fig. 3). Although the specificity of some of the antibodies for Piezo channels used previously was questionable, antibodies with improved characteristics have been developed in the past few years. Our data indicated that knockdown of Piezo channels with siRNA dramatically reduced staining and strengthened support for these antibodies (Fig. S3). Additional support from others validates the staining of the antibodies used in this study, including KO mice models, reporter mice, pre-absorption assay, or genetically modified cell lines [50-57].

Investigating the early reactions of RGCs and their microenvironment to initial stressors is pivotal for understanding the pathogenesis of glaucoma. To our knowledge, this is the first study to identify both baseline and scotopic response changes with Piezo1 activation in the retina, using MEA recording. Increases in excitability drive greater energy demand and can lead to a greater accumulation of metabolic by-products, including reactive oxygen species, from mitochondrial ATP production trying to mitigate the energy imbalance of the RGCs, which in turn may lead to RGC dysfunction [70]. Similar emergence of spontaneous hyperactivity in RGCs has also been detected in animal models of retinal degeneration as the disease progress [71-74]. Speculations concerning the impact of spontaneous hyperactivity among RGCs on patients' vision suggest an increase in background noise, potentially disrupting the transmission of normal signals essential for visual perception when processed by various brain circuits. Ultimately, this could lead to a reduced signal-to-noise ratio, characterized by a higher rate of action potentials discharged by ganglion cells [75,76]. Piezo1, a mechanically activated ion channel, has been implicated in various physiological processes, including cellular mechanotransduction. In the context of glaucoma, where increased intraocular pressure can lead to mechanical stress on RGCs, Piezo1 could be a critical factor in how these cells adapt to preserve their function or mitigate stress and could potentially open up new avenues for therapeutic strategies targeting RGC protection and

neuroprotection, which may complement IOP-lowering treatments and improve outcomes for patients with glaucoma. With no available specific Piezo2 agonist, its involvement cannot be ruled out, as they may have overlapping functions.

The observations above contribute to the understanding of Piezo1 and 2 channels in the posterior eye, confirming some, but not all, previous findings. For example, staining for Piezo2 was quite evenly distributed throughout the retina in an earlier study on mice, although Piezo1 showed some concentration in the ganglion cell layer [24]. In the guinea pig retina, staining of Piezo1 is also expressed throughout the retina [25]. A recent study using fluorescent in situ hybridization to overcome issues with earlier antibodies found mRNA for *Piezo1* in selected regions of the mouse ganglion cell layer and inner nuclear layer, although expression of *Piezo2* message was more restricted [27]. This difference is not unexpected, however, as the highest antigen signal in our study was from the axons where mRNA levels are likely quite low. RNA messages for *Piezo1* and *Piezo2* were previously reported in mouse optic nerve head tissue and in 22% and 43%, respectively, of isolated optic nerve head astrocytes [77]; while our immunostaining suggests a higher level of expression in cultured optic nerve head astrocytes, this may reflect differences in culture protocols. In a more recent study, Yoda1 increased fibronectin and Ca^{2+} levels in mouse optic nerve head astrocytes with Piezo1, but not Piezo2, localized to optic nerve head astrocytes and increased by stretch [78], although this study was exclusively in vitro. Addition of Yoda1 and increased hydrostatic pressure-activated currents and Ca^{2+} transients in retinal capillary cells [26]; although we did not notice any staining in retinal capillary cells, their detection is best done in wholemounts, and we largely used sections, so cannot rule them out.

Implications for pathology, neuron growth, and interactions with other mechanosensitive channels.

The identification of both Piezo1 and Piezo2 on axons of RGCs as they pass through optic nerve head has direct relevance in glaucoma, as elevated IOP distorts lamina cribrosa of the optic

nerve head, causing damage to the axons [79], and axonal neuropathy of RGCs is an early sign of glaucomatous damage [80,81]. While the role of Piezo channels in this mechanosensitive damage is unclear, their substantial presence in healthy axons suggests a protective contribution under homeostatic conditions. Excessive stimulation may be damaging, however, and the sustained influx of Ca^{2+} is pathological to neurons. Aberrant Ca^{2+} signaling recently indicated dysfunctional cortical signaling after mild traumatic brain injury [82], and can disrupt axonal transport [83]. As mitochondrial dysfunction plays a central role in RGC loss [84], recent reports of the activation of mitochondria by Piezo1 may have relevance [85].

In addition, the mechanosensitive release of ATP through pannexin hemichannels is implicated after stretch and in eyes with elevated IOP [86-88], and stimulation of the P2X7 receptor for ATP can activate microglial cells and injure neurons [41,89]. Piezo channels can trigger ATP release from red blood cells [90] and interact with pannexin channels in cholangiocytes [91], although a Piezo-pannexin-ATP link in the optic nerve head remains to be determined. Recent evidence that repeated elevations in IOP can lead to inflammation following activation of the pannexin1 channel supports this link [92]. The inflammatory responses accompanying the elevation of IOP are substantial, suggesting a possible upstream role for Piezo channels [93,94].

Elevation of both *Piezo1* and *Piezo2* after stretch *in vivo* may have implications for pathology. Mechanical forces influence expression of Piezo channels; expression of Piezo1 channels in stem cells was increased with substrate stiffness [95], while Piezo1 levels in myofibroblasts were increased with 18 or 24 hours of 10% stretch [96]. In the optic nerve head, expression of Piezo2, but not Piezo1, was upregulated in the DBA/2J mouse model of glaucoma at 10 [77] or 15 months [24], although the strain was relatively continuous in this model. A two-hour 10% stretch doubled Piezo1 expression in mouse optic nerve head astrocytes [78]. An ischemia-perfusion model in which IOP was raised to 100 mmHg increased Piezo2 expression at 3 and 5 days, with a return to baseline at 7 days [24], while elevating IOP to 30 mmHg for 1 hr did not alter

Piezo1 or 2 expression [77]. The sustained rise in Piezo expression detected in this study suggests the CEI model of ocular hypertension, where IOP is increased to 60 mmHg to generate a non-ischemic pressure rise, produces a sufficient tissue stretch to upregulate Piezo expression. Similar upregulation of specialized excitatory channels, NaV1.6 [65] and Trpv1 [97],has also been reported, accompanying a chronic rise in IOP. The ability of a single episode of tissue stretch to induce a prolonged rise in Piezo channel expression suggests a mechanism where neural tissue becomes increasingly sensitive to mechanical stain with repeated stimulation. This has implications for brains exposed to repeated traumatic injury, and for eyes exposed to multiple spikes in IOP, as an increase in Piezo expression could increase the Ca^{2+} entry, with negative consequences for neurons.

While Piezo1 has been implicated in the growth of RGC axons, the nature of this influence remains to be determined as inhibition of mechanosentitive channels with GsMTx4 and knockdown of Piezo1 reduced RGC axon growth in Xenopus [98], but GsMTx4 increased growth of mouse RGC neurites in culture and Piezo1 agonist Yoda1 reduced their growth [24]. The role of Piezo channels in the retina may vary with age, as Piezo1 levels were higher in the optic nerve head of neonatal mice than in 3-month-old mice; cultured astrocytes with Piezo1 knocked down showed decreased expression of cytoskeletal and cell cycle genes, suggesting a role in development [99]. The results from cultured cells above may reflect developmental influences on the cells. Regardless, the presence of Piezo1 on RGC axons in mice 3-6 months of age implies the channel has additional contributions to the homeostatic functions of adult RGCs.

In addition to its own mechanosensitive activity, Piezo channels may also influence the activity of other channels. Piezo channel opening contributes to the mechanosensitive current through TREK-1 channels [100], while Piezo1 was identified as the upstream mechanosensor that connects shear stress to TRPV4 opening in endothelial cells [101,102]. This could help the transient opening of the Piezo channel pore to drive a more sustained response, particularly at higher levels of strain [103]. Similar interactions between Piezo channels and TRPV4 would have relevance in

the retina, where TRPV4 has long been implicated in mechanosensitive responses [104-106]. Müller cells showed strong expression of mRNA for both Piezo1 and TRPV4, and the mechanosensitive elevation in Ca^{2+} was only partially reduced in TRPV4$^{-/-}$ mice, suggesting Piezo1 channels may interact with TRPV4 in the mechanosensitive responses of Müller cells [107]. The Ca^{2+} elevation induced by mechanical strain initiated in the end feet region; while the colocalization of Piezo1 with glutamine synthetase on Müller cell end feet above supports an interaction, more research is needed.

Conclusions

In summary, this study has identified both Piezo1 and Piezo2 channels in mouse, rat and in human iPSC-RGCs, with expression in soma and axons. Functional assays confirmed the presence of Piezo1 in the soma and neurites of the neurons. Activation of the Piezo1 channel in the explant retina increased RGC excitability at both baseline and scotopic conditions. Sustained elevation of *Piezo1* and *Piezo2* occurred after a single transient stretch. The presence of both Piezo1 and Piezo2 on the axons and soma, and the sustained rise in Piezo expression after a single exposure to stretch may provide a mechanism for enhanced neural sensitivity to repeated insults in pathologies like glaucoma or traumatic brain injury.

Acknowledgements

The authors would like to thank Hydar Ali for his generous access to his Varioskan device. This study was supported by R01 EY015537, R01 EY015537S1, R01 EY013434, P30 EY001583, R01 EY023557, Research to Prevent Blindness Unrestricted Grant, Penn Health-Tech Seed Funding.

Conflict of Interest

All the authors have read the manuscript and declare no conflict of interest.

Author contributions

PS made substantial contributions to the conception and design of the work, the acquisition, analysis and interpretation of data, and drafted and edited the work; LS made substantial contributions to the conception and design of the work, and the acquisition; SN made substantial contributions to acquisition, analysis and interpretation of data; VRMC made substantial contributions to the acquisition of data; VV made substantial contributions to the acquisition of data; JH made substantial contributions to the acquisition of data, JMOB made substantial contributions to the acquisition of data; JX made substantial contributions to the acquisition of data, analysis and interpretation of data; WL made substantial contributions to the conception and design of the work, the acquisition, analysis and interpretation of data; CHM made substantial contributions to the conception and design of the work, analysis and interpretation of data, and drafted and edited the work. All authors have approved the submitted version and agreed both to be personally accountable for the author's own contributions and to ensure that questions related to the accuracy or integrity of any part of the work, are appropriately investigated, resolved, and the resolution documented in the literature.

Data Availability statement

All data generated or analyzed during this study are included in this manuscript and its supplementary information files, or are available from the corresponding author upon reasonable request.

References:

1. Yang Qq, Zhou Jw. Neuroinflammation in the central nervous system: Symphony of glial cells. *Glia*. 2019;67(6):1017-1035.
2. Keating CE, Cullen DK. Mechanosensation in traumatic brain injury. *Neurobiol Dis*. Jan 2021;148:105210. doi:10.1016/j.nbd.2020.105210
3. DiSabato DJ, Quan N, Godbout JP. Neuroinflammation: the devil is in the details. *Journal of neurochemistry*. 2016;139:136-153.
4. Gilhus NE, Deuschl G. Neuroinflammation—a common thread in neurological disorders. *Nature Reviews Neurology*. 2019;15(8):429-430.
5. Coste B, Mathur J, Schmidt M, et al. Piezo1 and Piezo2 are essential components of distinct mechanically activated cation channels. *Science*. Oct 1 2010;330(6000):55-60. doi:10.1126/science.1193270
6. Guo YR, MacKinnon R. Structure-based membrane dome mechanism for Piezo mechanosensitivity. *eLife*. 2017/12/12 2017;6:e33660. doi:10.7554/eLife.33660
7. Volkers L, Mechioukhi Y, Coste B. Piezo channels: from structure to function. *Pflügers Archiv-European Journal of Physiology*. 2015;467:95-99.
8. Wu J, Lewis AH, Grandl J. Touch, tension, and transduction–the function and regulation of Piezo ion channels. *Trends in biochemical sciences*. 2017;42(1):57-71.
9. Gnanasambandam R, Bae C, Gottlieb PA, Sachs F. Ionic Selectivity and Permeation Properties of Human PIEZO1 Channels. *PLoS One*. 2015;10(5):e0125503. doi:10.1371/journal.pone.0125503
10. De Felice D, Alaimo A. Mechanosensitive Piezo Channels in Cancer: Focus on altered Calcium Signaling in Cancer Cells and in Tumor Progression. *Cancers (Basel)*. Jul 3 2020;12(7)doi:10.3390/cancers12071780
11. Dalghi MG, Ruiz WG, Clayton DR, et al. Functional roles for PIEZO1 and PIEZO2 in urothelial mechanotransduction and lower urinary tract interoception. *JCI insight*. 2021;6(19)
12. Glogowska E, Arhatte M, Chatelain FC, et al. Piezo1 and Piezo2 foster mechanical gating of K2P channels. *Cell Reports*. 2021;37(9)
13. Delmas P, Parpaite T, Coste B. PIEZO channels and newcomers in the mammalian mechanosensitive ion channel family. *Neuron*. 2022;110(17):2713-2727.
14. Qiu Z, Guo J, Kala S, et al. The mechanosensitive ion channel Piezo1 significantly mediates in vitro ultrasonic stimulation of neurons. *Iscience*. 2019;21:448-457.
15. Song Y, Li D, Farrelly O, et al. The mechanosensitive ion channel piezo inhibits axon regeneration. *Neuron*. 2019;102(2):373-389. e6.
16. Li F, Lo TY, Miles L, et al. The Atr-Chek1 pathway inhibits axon regeneration in response to Piezo-dependent mechanosensation. *Nature communications*. 2021;12(1):3845.
17. Li J, Zhang Y, Lou Z, et al. Magnetic Nanobubble Mechanical Stress Induces the Piezo1-Ca2+-BMP2/Smad Pathway to Modulate Neural Stem Cell Fate and MRI/Ultrasound Dual Imaging Surveillance for Ischemic Stroke. *Small*. 2022;18(23):2201123.
18. Jasien JV, Fazio MA, Samuels BC, Johnston JM, Downs JC. Quantification of Translaminar Pressure Gradient (TLPG) With Continuous Wireless Telemetry in

Nonhuman Primates (NHPs). *Transl Vis Sci Technol*. Nov 2020;9(12):18. doi:10.1167/tvst.9.12.18
19. Downs JC, Roberts MD, Burgoyne CF. The mechanical environment of the optic nerve head in glaucoma. *Optometry and vision science: official publication of the American Academy of Optometry*. 2008;85(6):425.
20. Quigley HA, Addicks EM, Green WR, Maumenee A. Optic nerve damage in human glaucoma: II. The site of injury and susceptibility to damage. *Archives of ophthalmology*. 1981;99(4):635-649.
21. Križaj D, Ryskamp DA, Tian N, et al. From mechanosensitivity to inflammatory responses: new players in the pathology of glaucoma. *Current eye research*. 2014;39(2):105-119.
22. Sommer A. Intraocular pressure and glaucoma. *American journal of ophthalmology*. 1989;107(2):186-188.
23. Wiggs JL. The cell and molecular biology of complex forms of glaucoma: updates on genetic, environmental, and epigenetic risk factors. *Investigative ophthalmology & visual science*. 2012;53(5):2467-2469.
24. Morozumi W, Inagaki S, Iwata Y, Nakamura S, Hara H, Shimazawa M. Piezo channel plays a part in retinal ganglion cell damage. *Experimental eye research*. 2020;191:107900.
25. Zhong W, Lan C, Gu Z, et al. The Mechanosensitive Piezo1 Channel Mediates Mechanochemical Transmission in Myopic Eyes. *Investigative Ophthalmology & Visual Science*. 2023;64(7):1-1.
26. Harraz OF, Klug NR, Senatore AJ, Hill-Eubanks DC, Nelson MT. Piezo1 Is a Mechanosensor Channel in Central Nervous System Capillaries. *Circ Res*. May 13 2022;130(10):1531-1546. doi:10.1161/circresaha.122.320827
27. Zhu Y, Garcia-Sanchez J, Dalal R, et al. Differential expression of PIEZO1 and PIEZO2 mechanosensitive channels in ocular tissues implicates diverse functional roles. *Exp Eye Res*. Oct 10 2023;236:109675. doi:10.1016/j.exer.2023.109675
28. Liu WW, Kinzy TG, Cooke Bailey JN, et al. Mechanosensitive ion channel gene survey suggests potential roles in primary open angle glaucoma. *Scientific Reports*. 2023/09/23 2023;13(1):15871. doi:10.1038/s41598-023-43072-3
29. Chavali VRM, Haider N, Rathi S, et al. Dual SMAD inhibition and Wnt inhibition enable efficient and reproducible differentiations of induced pluripotent stem cells into retinal ganglion cells. *Sci Rep*. Jul 16 2020;10(1):11828. doi:10.1038/s41598-020-68811-8
30. Xia J, Lim JC, Lu W, et al. Neurons respond directly to mechanical deformation with pannexin-mediated ATP release and autostimulation of P2X7 receptors. *The Journal of Physiology*. 2012;590(10):2285-2304. doi:10.1113/jphysiol.2012.227983
31. Wang L, Klingeborn M, Travis AM, Hao Y, Arshavsky VY, Gospe SM, 3rd. Progressive optic atrophy in a retinal ganglion cell-specific mouse model of complex I deficiency. *Sci Rep*. Oct 1 2020;10(1):16326. doi:10.1038/s41598-020-73353-0
32. Winzeler A, Wang JT. Purification and culture of retinal ganglion cells from rodents. *Cold Spring Harb Protoc*. Jul 1 2013;2013(7):643-52. doi:10.1101/pdb.prot074906
33. Lim JC, Lu W, Beckel JM, Mitchell CH. Neuronal release of cytokine IL-3 triggered by mechanosensitive autostimulation of the P2X7 receptor Is neuroprotective.

Front Cell Neurosci. 2016;10:270. PMID: 27932954 PMC5120082. doi:10.3389/fncel.2016.00270
34. Chen Y, Stevens B, Chang J, Milbrandt J, Barres BA, Hell JW. NS21: re-defined and modified supplement B27 for neuronal cultures. *J Neurosci Methods*. Jun 30 2008;171(2):239-47. doi:10.1016/j.jneumeth.2008.03.013
35. Albalawi F, Lu W, Beckel JM, Lim JC, McCaughey SA, CH M. The P2X7 receptor primes IL-1β and the NLRP3 inflammasome in astrocytes exposed to mechanical strain *Front Cell Neurosci*. 2017;11:227. . PMID:28848393 PMC5550720.
36. Gaub BM, Berry MH, Holt AE, et al. Restoration of visual function by expression of a light-gated mammalian ion channel in retinal ganglion cells or ON-bipolar cells. *Proceedings of the National Academy of Sciences*. 2014;111(51):E5574-E5583.
37. Song JY, Aravand P, Nikonov S, et al. Amelioration of neurosensory structure and function in animal and cellular models of a congenital blindness. *Molecular Therapy*. 2018;26(6):1581-1593.
38. Gómez NM, Lu W, Lim J, et al. Robust lysosomal calcium signaling through channel TRPML1 is impaired by lipofuscin accumulation *Faseb J*. 2018;32(2):782-794 PMID:29030399 PMC5888396. doi:doi: 10.1096/fj.201700220RR
39. Morrison JC, Cepurna WO, Tehrani S, et al. A period of controlled elevation of IOP (CEI) produces the specific gene expression responses and focal injury pattern of experimental rat glaucoma. *Investigative ophthalmology & visual science*. 2016;57(15):6700-6711.
40. Lu W, Albalawi F, Beckel JM, Lim JC, Laties AM, Mitchell CH. The P2X7 receptor links mechanical strain to cytokine IL-6 up-regulation and release in neurons and astrocytes. *J Neurochem*. 2017;141(3):436-448. PMID: 28244110 PMC5408351. PMID:28244110 PMC5408351 doi:10.1111/jnc.13998
41. Campagno KE, Lu W, Jassim AH, et al. Rapid morphologic changes to microglial cells and upregulation of mixed microglial activation state markers induced by P2X7 receptor stimulation and increased intraocular pressure. *J Neuroinflammation*. Sep 20 2021;18(1):217. doi:10.1186/s12974-021-02251-7
42. Zhi Z, Cepurna WO, Johnson EC, Morrison JC, Wang RK. Impact of intraocular pressure on changes of blood flow in the retina, choroid, and optic nerve head in rats investigated by optical microangiography. *Biomed Opt Express*. Sep 1 2012;3(9):2220-33. doi:10.1364/boe.3.002220
43. Kong YX, van Bergen N, Bui BV, et al. Impact of aging and diet restriction on retinal function during and after acute intraocular pressure injury. *Neurobiol Aging*. Jun 2012;33(6):1126.e15-25. doi:10.1016/j.neurobiolaging.2011.11.026
44. Crowston JG, Kong YXG, Trounce IA, et al. An acute intraocular pressure challenge to assess retinal ganglion cell injury and recovery in the mouse. *Experimental eye research*. 2015;141:3-8.
45. Lu W, Reigada D, Sevigny J, Mitchell CH. Stimulation of the P2Y1 receptor up-regulates nucleoside-triphosphate diphosphohydrolase-1 in human retinal pigment epithelial cells. *J Pharmacol Exp Ther*. Oct 2007;323(1):157-64. doi:jpet.107.124545 [pii]
10.1124/jpet.107.124545

46. Sigal IA, Flanagan JG, Tertinegg I, Ethier CR. Predicted extension, compression and shearing of optic nerve head tissues. *Exp Eye Res*. Sep 2007;85(3):312-22. doi:10.1016/j.exer.2007.05.005
47. Girard MJA, Suh J-KF, Bottlang M, Burgoyne CF, Downs JC. Biomechanical Changes in the Sclera of Monkey Eyes Exposed to Chronic IOP Elevations. *Investigative Ophthalmology & Visual Science*. 2011;52(8):5656-5669. doi:10.1167/iovs.10-6927
48. Lozano DC, Jayaram H, Cepurna WO, et al. Optic Nerve Head Gene Transcription Sequelae to a Single Elevated IOP Exposure Provides Insights Into Known Responses to Chronically Elevated IOP. *Investigative Ophthalmology & Visual Science*. 2023;64(10):4-4. doi:10.1167/iovs.64.10.4
49. Syeda R, Xu J, Dubin AE, et al. Chemical activation of the mechanotransduction channel Piezo1. *eLife*. 2015/05/22 2015;4:e07369. doi:10.7554/eLife.07369
50. Florez-Paz D, Bali KK, Kuner R, Gomis A. A critical role for Piezo2 channels in the mechanotransduction of mouse proprioceptive neurons. *Scientific Reports*. 2016;6(1):25923.
51. Narayanan P, Sondermann J, Rouwette T, et al. Native Piezo2 interactomics identifies pericentrin as a novel regulator of Piezo2 in somatosensory neurons. *Journal of Proteome Research*. 2016;15(8):2676-2687.
52. Jiang L, Zhao Y-d, Chen W-x. The function of the novel mechanical activated ion channel Piezo1 in the human osteosarcoma cells. *Medical Science Monitor: International Medical Journal of Experimental and Clinical Research*. 2017;23:5070.
53. Huo L, Gao Y, Zhang D, et al. Piezo2 channel in nodose ganglia neurons is essential in controlling hypertension in a pathway regulated directly by Nedd4-2. *Pharmacological Research*. 2021;164:105391.
54. Kulkarni S, Marquez J, Date P, Ventrella R, Mitchell BJ, Khokha MK. Mechanical stretch scales centriole number to apical area via Piezo1 in multiciliated cells. *Elife*. 2021;10:e66076.
55. Lee W, Nims RJ, Savadipour A, et al. Inflammatory signaling sensitizes Piezo1 mechanotransduction in articular chondrocytes as a pathogenic feed-forward mechanism in osteoarthritis. *Proceedings of the National Academy of Sciences*. 2021;118(13):e2001611118.
56. Dela Justina V, de Freitas RA, Arishe OO, Giachini FR, Webb RC, Priviero F. Piezo1 activation induces relaxation of the pudendal artery and corpus cavernosum. *Frontiers in Physiology*. 2023;14:168.
57. Madar J, Tiwari N, Smith C, et al. Piezo2 regulates colonic mechanical sensitivity in a sex specific manner in mice. *Nature Communications*. 2023;14(1):2158.
58. Riepe RE, Norenburg MD. Müller cell localisation of glutamine synthetase in rat retina. *Nature*. 1977/08/01 1977;268(5621):654-655. doi:10.1038/268654a0
59. Kwong JM, Caprioli J, Piri N. RNA binding protein with multiple splicing: a new marker for retinal ganglion cells. *Investigative ophthalmology & visual science*. 2010;51(2):1052-1058.
60. Jiang S-M, Zeng L-P, Zeng J-H, Tang L, Chen X-M, Wei X. β-III-Tubulin: a reliable marker for retinal ganglion cell labeling in experimental models of glaucoma. *International journal of ophthalmology*. 2015;8(4):643.

61. Nadal-Nicolás FM, Jiménez-López M, Sobrado-Calvo P, et al. Brn3a as a marker of retinal ganglion cells: qualitative and quantitative time course studies in naive and optic nerve-injured retinas. *Invest Ophthalmol Vis Sci*. Aug 2009;50(8):3860-8. doi:10.1167/iovs.08-3267
62. Yang Z, Wang KK. Glial fibrillary acidic protein: from intermediate filament assembly and gliosis to neurobiomarker. *Trends Neurosci*. Jun 2015;38(6):364-74. doi:10.1016/j.tins.2015.04.003
63. Gudiseva HV, Vrathasha V, He J, Bungatavula D, O'Brien JM, Chavali VRM. Single Cell Sequencing of Induced Pluripotent Stem Cell Derived Retinal Ganglion Cells (iPSC-RGC) Reveals Distinct Molecular Signatures and RGC Subtypes. *Genes (Basel)*. Dec 18 2021;12(12)doi:10.3390/genes12122015
64. Basavarajappa D, Galindo-Romero C, Gupta V, et al. Signalling pathways and cell death mechanisms in glaucoma: Insights into the molecular pathophysiology. *Molecular Aspects of Medicine*. 2023;94:101216.
65. Risner ML, Pasini S, Cooper ML, Lambert WS, Calkins DJ. Axogenic mechanism enhances retinal ganglion cell excitability during early progression in glaucoma. *Proceedings of the National Academy of Sciences*. 2018;115(10):E2393-E2402.
66. Tao X, Sabharwal J, Wu SM, Frankfort BJ. Intraocular pressure elevation compromises retinal ganglion cell light adaptation. *Investigative Ophthalmology & Visual Science*. 2020;61(12):15-15.
67. Lee W, Leddy HA, Chen Y, et al. Synergy between Piezo1 and Piezo2 channels confers high-strain mechanosensitivity to articular cartilage. *Proceedings of the National Academy of Sciences*. 2014;111(47):E5114-E5122.
68. Zhou T, Gao B, Fan Y, et al. Piezo1/2 mediate mechanotransduction essential for bone formation through concerted activation of NFAT-YAP1-ß-catenin. *eLife*. 2020/03/18 2020;9:e52779. doi:10.7554/eLife.52779
69. Swain SM, Liddle RA. Piezo1 acts upstream of TRPV4 to induce pathological changes in endothelial cells due to shear stress. *Journal of Biological Chemistry*. 2021;296
70. Smith BJ, McHugh CF, Hirano AA, Brecha NC, Barnes S. Transient and sustained ganglion cell light responses are differentially modulated by intrinsically produced reactive oxygen species acting upon specific voltage-gated Na+ channel isoforms. *Journal of Neuroscience*. 2023;43(13):2291-2304.
71. Dräger UC, Hubel DH. Studies of visual function and its decay in mice with hereditary retinal degeneration. *Journal of Comparative Neurology*. 1978;180(1):85-114.
72. Stasheff SF. Emergence of Sustained Spontaneous Hyperactivity and Temporary Preservation of Off Responses in Ganglion Cells of the Retinal Degeneration (rd1) Mouse. *Journal of Neurophysiology*. 2008;99(3):1408-1421. doi:10.1152/jn.00144.2007
73. Stasheff SF. Clinical Impact of Spontaneous Hyperactivity in Degenerating Retinas: Significance for Diagnosis, Symptoms, and Treatment. *Frontiers in cellular neuroscience*. 2018;12:298. doi:10.3389/fncel.2018.00298 Accessed 2018.
74. Goo YS, Park DJ, Ahn JR, Senok SS. Spontaneous oscillatory rhythms in the degenerating mouse retina modulate retinal ganglion cell responses to electrical stimulation. *Frontiers in cellular neuroscience*. 2016;9:512.

75. Ivanova E, Yee CW, Sagdullaev BT. Increased phosphorylation of Cx36 gap junctions in the AII amacrine cells of RD retina. *Frontiers in cellular neuroscience*. 2015;9:390.
76. Barrett JM, Degenaar P, Sernagor E. Blockade of pathological retinal ganglion cell hyperactivity improves optogenetically evoked light responses in rd1 mice. *Frontiers in cellular neuroscience*. 2015;9:330.
77. Choi HJ, Sun D, Jakobs TC. Astrocytes in the optic nerve head express putative mechanosensitive channels. *Molecular vision*. 2015;21:749.
78. Liu J, Yang Y, Liu Y. Piezo1 plays a role in optic nerve head astrocyte reactivity. *Experimental eye research*. 2021;204:108445.
79. Quigley HA, Hohman RM, Addicks EM, Massof RW, Green WR. Morphologic changes in the lamina cribrosa correlated with neural loss in open-angle glaucoma. *American journal of ophthalmology*. 1983;95(5):673-691.
80. Howell GR, Libby RT, Jakobs TC, et al. Axons of retinal ganglion cells are insulted in the optic nerve early in DBA/2J glaucoma. *The Journal of cell biology*. 2007;179(7):1523-1537.
81. Chidlow G, Ebneter A, Wood JP, Casson RJ. The optic nerve head is the site of axonal transport disruption, axonal cytoskeleton damage and putative axonal regeneration failure in a rat model of glaucoma. *Acta neuropathologica*. 2011;121:737-751.
82. Cramer SW, Haley SP, Popa LS, et al. Wide-field calcium imaging reveals widespread changes in cortical functional connectivity following mild traumatic brain injury in the mouse. *Neurobiol Dis*. Jan 2023;176:105943. doi:10.1016/j.nbd.2022.105943
83. Prior R, Van Helleputte L, Benoy V, Van Den Bosch L. Defective axonal transport: A common pathological mechanism in inherited and acquired peripheral neuropathies. *Neurobiol Dis*. Sep 2017;105:300-320. doi:10.1016/j.nbd.2017.02.009
84. Muench NA, Patel S, Maes ME, Donahue RJ, Ikeda A, Nickells RW. The Influence of Mitochondrial Dynamics and Function on Retinal Ganglion Cell Susceptibility in Optic Nerve Disease. *Cells*. Jun 25 2021;10(7)doi:10.3390/cells10071593
85. Li X, Kordsmeier J, Nookaew I, Kim HN, Xiong J. Piezo1 stimulates mitochondrial function via cAMP signaling. *Faseb j*. Oct 2022;36(10):e22519. doi:10.1096/fj.202200300R
86. Lu W, Hu H, Sevigny J, et al. Rat, mouse, and primate models of chronic glaucoma show sustained elevation of extracellular ATP and altered purinergic signaling in the posterior eye. *Invest Ophthalmol Vis Sci*. May 2015;56(5):3075-83. doi:10.1167/iovs.14-15891
87. Zhang X, Li A, Ge J, Reigada D, Laties AM, Mitchell CH. Acute increase of intraocular pressure releases ATP into the anterior chamber. *Exp Eye Res*. Nov 2007;85(5):637-43. doi:S0014-4835(07)00206-0 [pii] 10.1016/j.exer.2007.07.016
88. Li A, Zhang X, Zheng D, Ge J, Laties AM, Mitchell CH. Sustained elevation of extracellular ATP in aqueous humor from humans with primary chronic angle-closure glaucoma. *Exp Eye Res*. Jul 2 2011;93(4):528-33 PMID:21745471 PMC3374644. doi:10.1016/j.exer.2011.06.020

89. Mitchell CH, Lu W, Hu H, Zhang X, Reigada D, Zhang M. The P2X(7) receptor in retinal ganglion cells: A neuronal model of pressure-induced damage and protection by a shifting purinergic balance. *Purinergic Signal*. Jun 2009;5(2):241-9 PMID 2686831PMCID 2583208. doi:10.1007/s11302-009-9142-6
90. Cinar E, Zhou S, DeCourcey J, Wang Y, Waugh RE, Wan J. Piezo1 regulates mechanotransductive release of ATP from human RBCs. *Proc Natl Acad Sci U S A*. Sep 22 2015;112(38):11783-8. doi:10.1073/pnas.1507309112
91. Desplat A, Penalba V, Gros E, Parpaite T, Coste B, Delmas P. Piezo1–Pannexin1 complex couples force detection to ATP secretion in cholangiocytes. *Journal of General Physiology*. 2021;153(12):e202112871.
92. Spurlock M, An W, Reshetnikova G, et al. The Inflammasome-Dependent Dysfunction and Death of Retinal Ganglion Cells after Repetitive Intraocular Pressure Spikes. *Cells*. 2023;12(22):2626.
93. Shestopalov VI, Spurlock M, Gramlich OW, Kuehn MH. Immune Responses in the Glaucomatous Retina: Regulation and Dynamics. *Cells*. Aug 3 2021;10(8)doi:10.3390/cells10081973
94. Wurl JA, Mac Nair CE, Dietz JA, Shestopalov VI, Nickells RW. Contralateral Astrocyte Response to Acute Optic Nerve Damage Is Mitigated by PANX1 Channel Activity. *Int J Mol Sci*. Oct 27 2023;24(21)doi:10.3390/ijms242115641
95. Chen X, Wanggou S, Bodalia A, et al. A Feedforward Mechanism Mediated by Mechanosensitive Ion Channel PIEZO1 and Tissue Mechanics Promotes Glioma Aggression. *Neuron*. 2018/11/21/ 2018;100(4):799-815.e7. doi:https://doi.org/10.1016/j.neuron.2018.09.046
96. He J, Fang B, Shan S, et al. Mechanical stretch promotes hypertrophic scar formation through mechanically activated cation channel Piezo1. *Cell Death Dis*. Mar 1 2021;12(3):226. doi:10.1038/s41419-021-03481-6
97. Weitlauf C, Ward NJ, Lambert WS, et al. Short-term increases in transient receptor potential vanilloid-1 mediate stress-induced enhancement of neuronal excitation. *Journal of Neuroscience*. 2014;34(46):15369-15381.
98. Koser DE, Thompson AJ, Foster SK, et al. Mechanosensing is critical for axon growth in the developing brain. *Nat Neurosci*. Dec 2016;19(12):1592-1598. doi:10.1038/nn.4394
99. Wan Y, Wang H, Fan X, et al. Mechanosensitive channel Piezo1 is an essential regulator in cell cycle progression of optic nerve head astrocytes. *Glia*. 2023;71(5):1233-1246.
100. Glogowska E, Arhatte M, Chatelain FC, et al. Piezo1 and Piezo2 foster mechanical gating of K2P channels. *Cell Reports*. 2021/11/30/ 2021;37(9):110070. doi:https://doi.org/10.1016/j.celrep.2021.110070
101. Swain SM, Liddle RA. Piezo1 acts upstream of TRPV4 to induce pathological changes in endothelial cells due to shear stress. *J Biol Chem*. Jan-Jun 2021;296:100171. doi:10.1074/jbc.RA120.015059
102. Swain SM, Liddle RA. Mechanosensing Piezo channels in gastrointestinal disorders. *The Journal of Clinical Investigation*. 10/02/ 2023;133(19)doi:10.1172/JCI171955

103. Zhang M, Meng N, Wang X, Chen W, Zhang Q. TRPV4 and PIEZO Channels Mediate the Mechanosensing of Chondrocytes to the Biomechanical Microenvironment. *Membranes (Basel)*. Feb 18 2022;12(2)doi:10.3390/membranes12020237
104. Ryskamp DA, Witkovsky P, Barabas P, et al. The polymodal ion channel transient receptor potential vanilloid 4 modulates calcium flux, spiking rate, and apoptosis of mouse retinal ganglion cells. *Journal of Neuroscience*. 2011;31(19):7089-7101.
105. Guarino BD, Paruchuri S, Thodeti CK. The role of TRPV4 channels in ocular function and pathologies. *Exp Eye Res*. Dec 2020;201:108257. doi:10.1016/j.exer.2020.108257
106. Redmon SN, Yarishkin O, Lakk M, et al. TRPV4 channels mediate the mechanoresponse in retinal microglia. *Glia*. Jun 2021;69(6):1563-1582. doi:10.1002/glia.23979
107. Jo AO, Lakk M, Rudzitis CN, Križaj D. TRPV4 and TRPC1 channels mediate the response to tensile strain in mouse Müller cells. *Cell Calcium*. 2022;104:102588.

Figures and legends

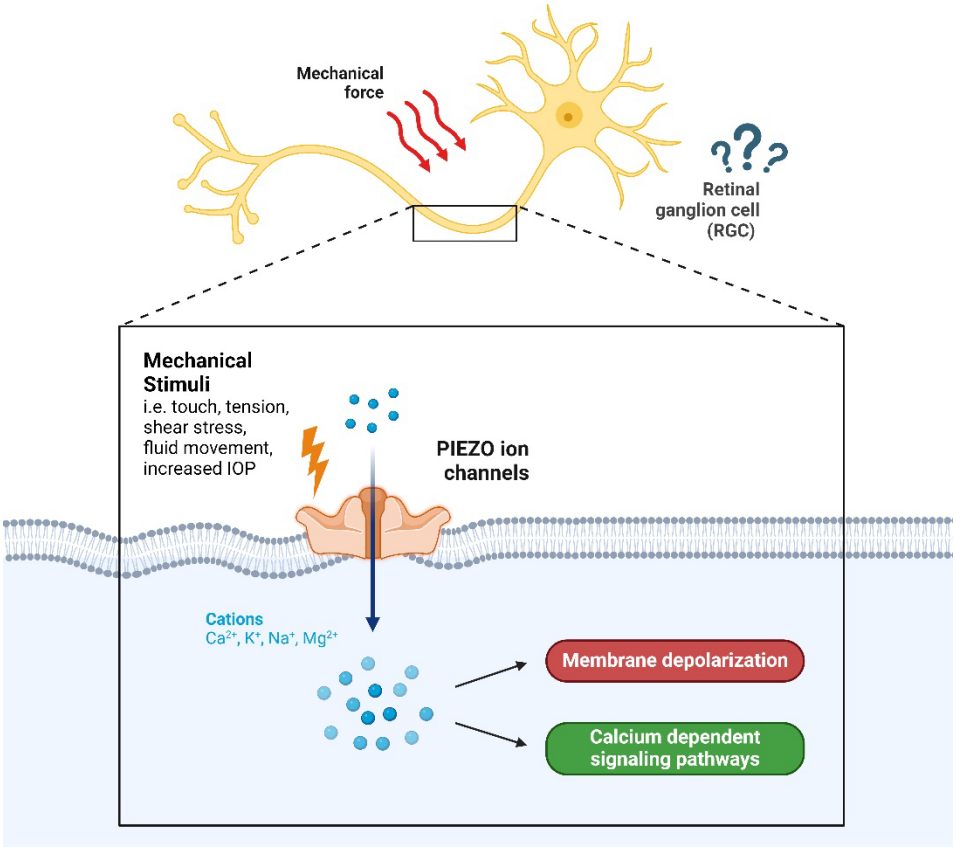

Graphical abstract

Piezo1 and Piezo2 channels in retinal ganglion cells and the impact of Piezo1 stimulation on light-dependent neural activity. Puttipong Sripinun, Lily P. See, Sergei Nikonov, Venkata Ramana Murthy Chavali, Vrathasha Vrathasha, Jie He, Joan M. O'Brien, Jingsheng Xia, Wennan Lu, Claire H. Mitchell*. Activation of Piezo channels through mechanical or pharmacological stimulation leads to an influx of Ca^{2+} and other cations into RGCs, depolarizing the membrane and increasing the action potential frequency to modulate the visual signal. Created with Biorender.com

Figure 1. Both mechanosensitive Piezo isoform genes are expressed in the mouse retina, optic nerve and RPE/choroid and were upregulated with transient IOP elevation *in vivo* at both 1 and 10 days. (A) Representative 2% agarose gel image of end-point PCR products of mRNA encoding *Piezo1* and *Piezo2*. *Gapdh* served as a loading control. **(B)** Semi-quantitative real-time PCR of *Piezo1* and *Piezo2* expression levels in different tissues in the eye normalized to neural retina. The relative expression of putative mechanosensitive ion channels was in agreement between PCR and semi-quantitative real-time PCR, where both *Piezo1* and *Piezo2* expression levels are expressed in all three types of tissues with greater prominent in RPE choroid and optic nerve tissue when compared to neural retina. (Unpaired t-test; n = 3; * p-value < 0.05, ** p-value < 0.01, *** p-value < 0.001). **(C, D)** Significant upregulation in the expression of both *Piezo1* and *Piezo2* was detected and maintained in recovery time points of 1 and 10 days in retinae exposed to elevated IOP in C57Bl/6J mice. **(E)** No changes were detected with sham needle insertion without elevation of intraocular pressure control group. Dots represent changes in expression from a single mouse, with expression normalized to the average ΔΔCT value of unpressurized contralateral eyes (paired Student's t-test, n = 6 mice per group).

Figure 2. Piezo1 activation altered scotopic RGC responses in retinal explant using MEA recording. (A) Representative light-evoked MEA records transitioning from Ames solution to Yoda1, where RGC demonstrated increases in spontaneous firing baseline and enhanced response to 337 photons s^{-1} μm^{-2} flashes of 455 nm light. **(B)** Average spontaneous firing rate of RGCs compared among three-time points. The spontaneous firing rate was increased when challenged by Yoda1 and decreased with the removal of Yoda1. (Repeated measures one-way ANOVA followed by Tukey's post-hoc test; n = 13 retina). **(C)** Representative light-evoked MEA recordings from control (left) and Yoda1 (right), where RGC demonstrated increases in spontaneous firing baseline and enhanced response to light of both ON- and OFF-responses can be observed. **(D)** On-transient responses from different retinal samples. (Paired t-test; n = 6-11 retina). **(E)** OFF transient responses from different retinal samples (Paired t-test; n = 6-10 retina). Statistical significance showed at * p-value < 0.05, ** p-value < 0.01, and **** p-value < 0.0001.

Figure 3. Calcium elevation triggered by specific Piezo1 agonist, Yoda1, in primary mouse RGCs and optic nerve head astrocytes (A1) tdTomato-labeled RGC isolated from *Slc17a6*$^{Cre+}$; *R26R*$^{tdTomato+}$ retina. **(A2)** Representative single-cell fura-2 Ca^{2+} imaging trace from a RGC soma in response to 50 μM Yoda1; the duration of drug application is indicated by the horizontal bar. **(A3)** Scatterplot of quantified Fura-2 peak in the response to Yoda1 at soma and neurite as comparison to baseline (Kruskal-Wallis test, n = 12-14; 7 biological replicates). **(A4)** Representative single-cell fura-2 Ca^{2+} imaging trace from a RGC soma in response to 50 μM Yoda1 with or without 3 μM Gd^{3+}; the duration of drug application is indicated by the horizontal bar. **(A5)** Scatterplot of quantified Fura-2 peak in the response to Yoda1 as comparison to baseline with or without 3 μM Gd^{3+} (One-way ANOVA tests followed by Tukey's post-hoc test; n = 6; 2 biological replicates). **(A6)** Scatterplot of quantified Fura-2 peak in the response to repeated Yoda1 exposure (One-way ANOVA tests followed by Tukey's post-hoc test; n = 5-6; 2 biological replicates). **(B1)** Isolated mouse optic nerve head astrocytes (MONHA) with immunocytochemistry confirmed expression of astrocyte marker, GFAP (green), and Piezo1 (red). **(B2)** Representative Fura-2 Ca^{2+} trace of optic nerve head astrocytes in response to 30 and 50 μM Yoda1 stimulation **(B3)** Scatterplot of quantified Fura-2 relative peak in response to Yoda1 in the astrocytes (One-way ANOVA tests followed by Tukey's post-hoc test, n = 8; 2 biological replicates).

Figure 4. Piezo1 channel immunoreactivity in the mouse retina overlaps with RGC, Müller cells and astrocyte markers: **(A)** Distribution of Piezo1 expression in the internal limiting membrane was highly co-localized with glutamine synthetase, a marker for Müller cells, at the

end feet compartments (white arrow). **(B, D)** Robust expression of Piezo1 in the retina in NFL and GCL. Double labeling with anti-Piezo1 and anti-beta-tubulin III antibodies showed positive staining in RGC. **(C)** Representative images of Piezo1 and BRN3A co-staining in the retina demonstrated a shared localization of both proteins in the RGCs' soma. **(E)** Positive staining of Piezo1 can be seen in the ONH area, where co-staining with GFAP representing astrocytes is evident at the glial lamina in the ONH. Here and throughout, NFL: Nerve fiber layer; GCL: Ganglion cell layer; IPL: Inner plexiform layer; INL: Inner nuclear layer; OPL: Outer plexiform layer; ONL: Outer nuclear layer. Images are representative of the staining found in 3 mice.

Figure 5. Piezo2 channel immunoreactivity in the mouse retina indicates strong expression in RGC axons: **(A)** Robust expression of Piezo2 in the retina in NFL and GCL. Double labeling with anti-Piezo2 and anti-beta-tubulin III antibodies shows strong colocalization from the soma and axons of RGCs in C57BL/6J eyes continued to the optic nerve after exiting the globe, with banding patterns evident. The staining pattern of the RGCs, especially dendrites and axons, is worth mentioning as a sharper characteristic compared to Piezo1 (white arrow). The inner nuclear layer displayed less staining for Piezo2 than for Piezo1. **(B)** Representative images of double immunolabeling Piezo2 and BRN3A in the retina demonstrated a shared localization of both proteins in the RGCs. Insets show magnified images of the regions enclosed by the white dashed boxes. Images representative of staining in 3 mice.

Figure 6 Expression of Piezo channels in iPSC-RGCs: **(A)** iPSC-RGCs were stained for pan retinal ganglion cell markers, Brn3A, and RBPMS to confirm the characterization. Scale bar, 50 µm. **(B)** Representative images showing positive staining of Piezo1 and Piezo2 in iPSC-RGCs confirm data from murine retinal tissues. Scale bar, 50 µm. **(C)** Representative images showing double immunostaining for Piezo2 and beta-tubulin III in iPSC-RGCs. Strong co-localization can be seen from the soma projecting toward the neurite of the cells (n=3; 2 biological replicates).

Figure 7. Long Evans rat retina shows similar immunoreactivity for Piezo1 and Piezo2 channels: **(A)** Reciprocal expression of Piezo1 to C57BL/6J eyes was recognized in the retina in NFL, GCL, and sparsely in INL. Double labeling with anti-Piezo1 and anti-beta-tubulin III antibodies show positive staining in RGCs' soma but not as strong as the end feet of Muller glial cells in the internal limiting membrane. Minimal staining at the RGC dendrites was also noted. Positive staining can also be seen in the ONH area. **(B)** Vigorous expression of Piezo2 in the retina in NFL and GCL. Co-staining with anti-Piezo2 and anti-beta-tubulin III antibodies shows strong colocalization from the soma and axons of RGCs, similarly as in C57BL/6J eyes continued to the optic nerve after exiting the globe. Pronounced expression at the dendrite of the RGCs was also presented. Insets show magnified images of the regions enclosed by the white dashed boxes. Images representative of staining in 3 rats.

Figure 1.

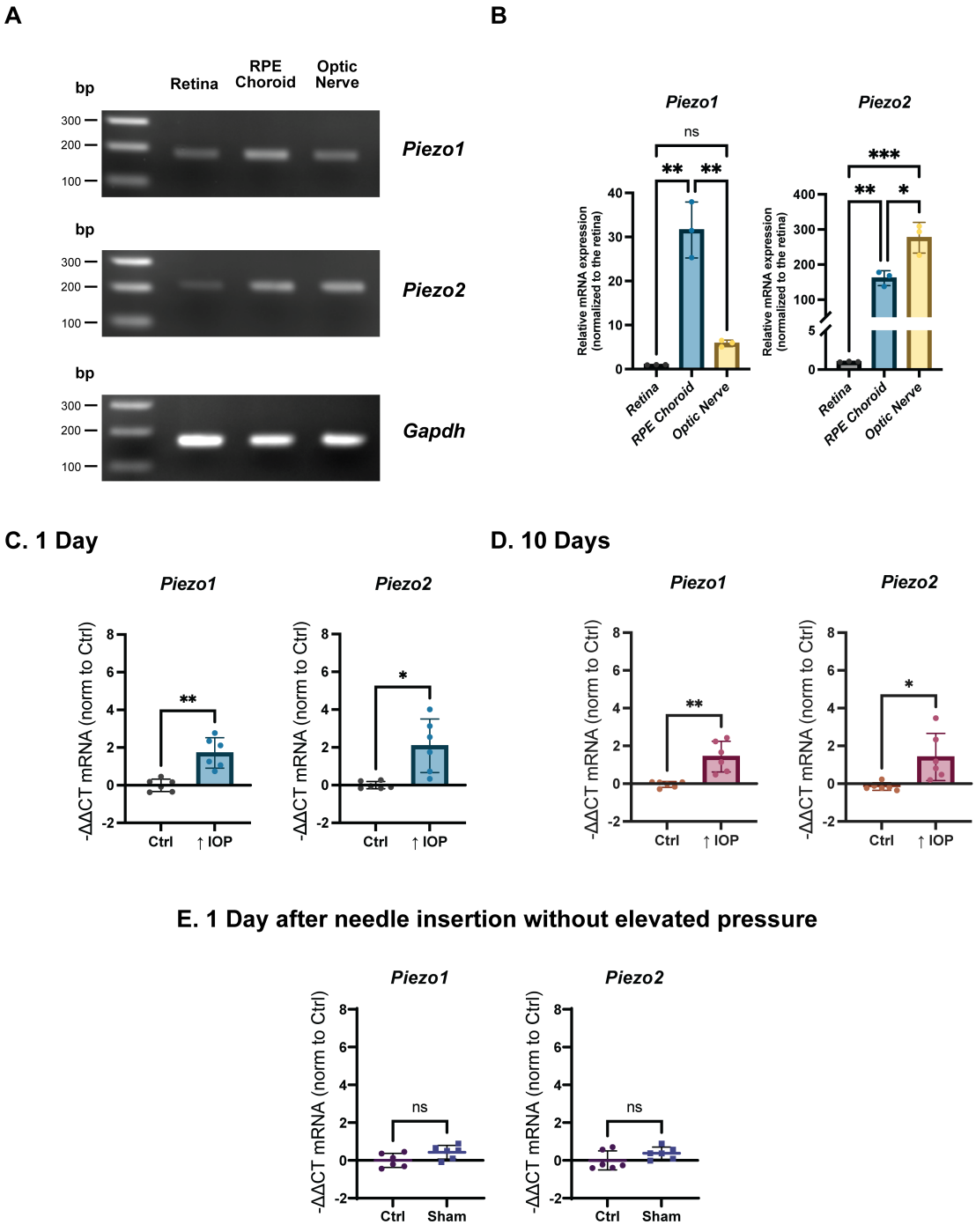

Figure 2.

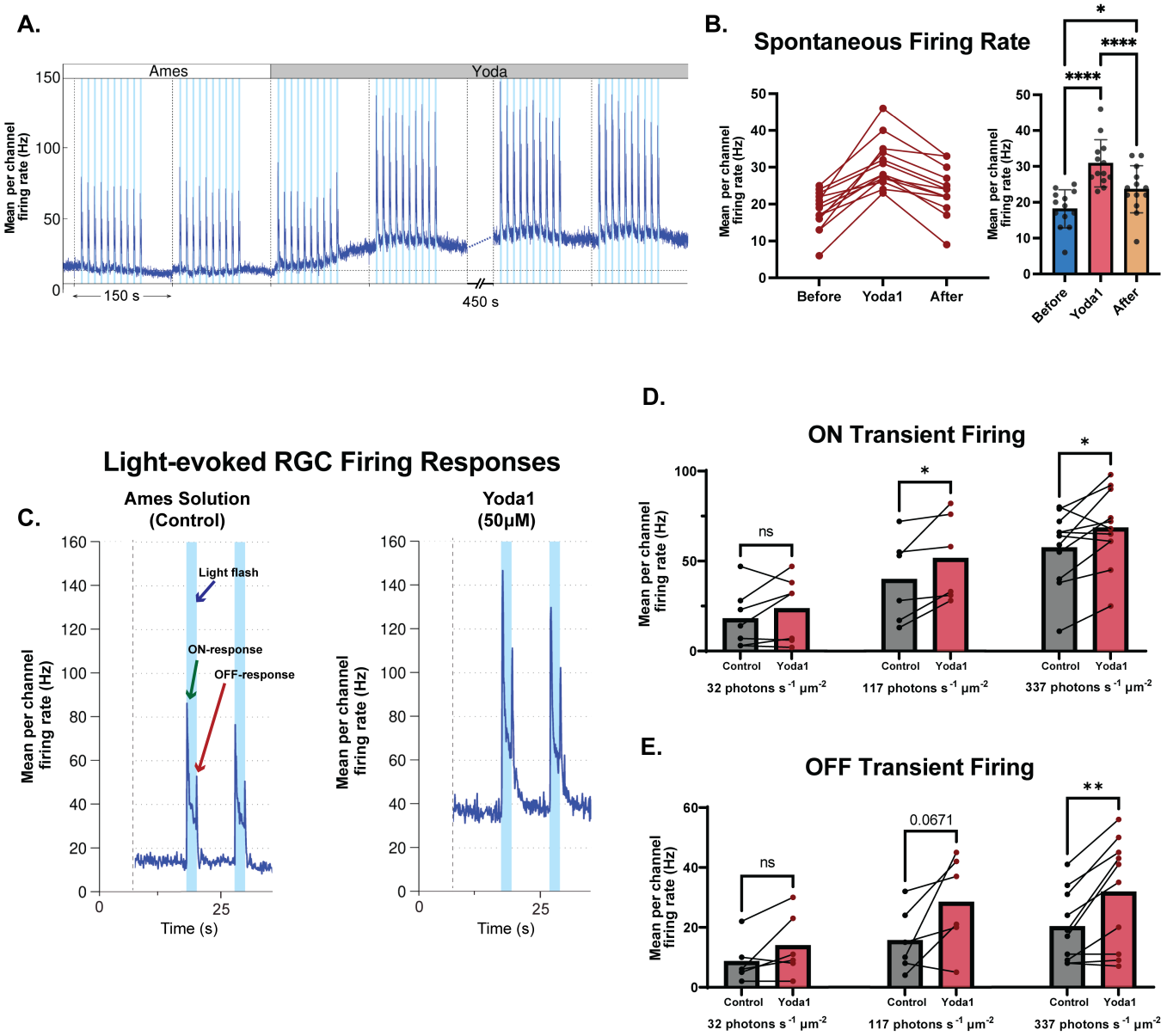

Figure 3.

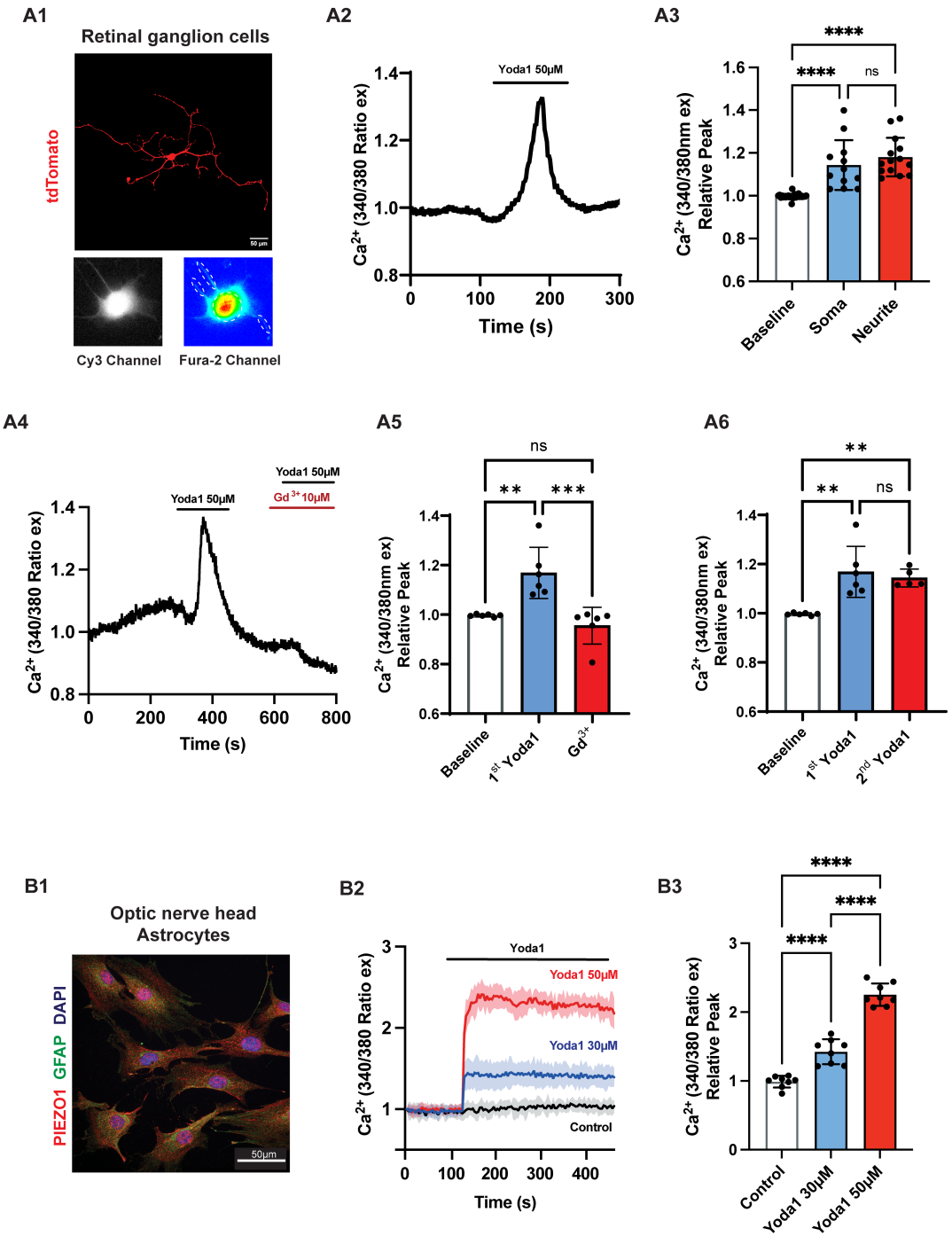

Figure 4.

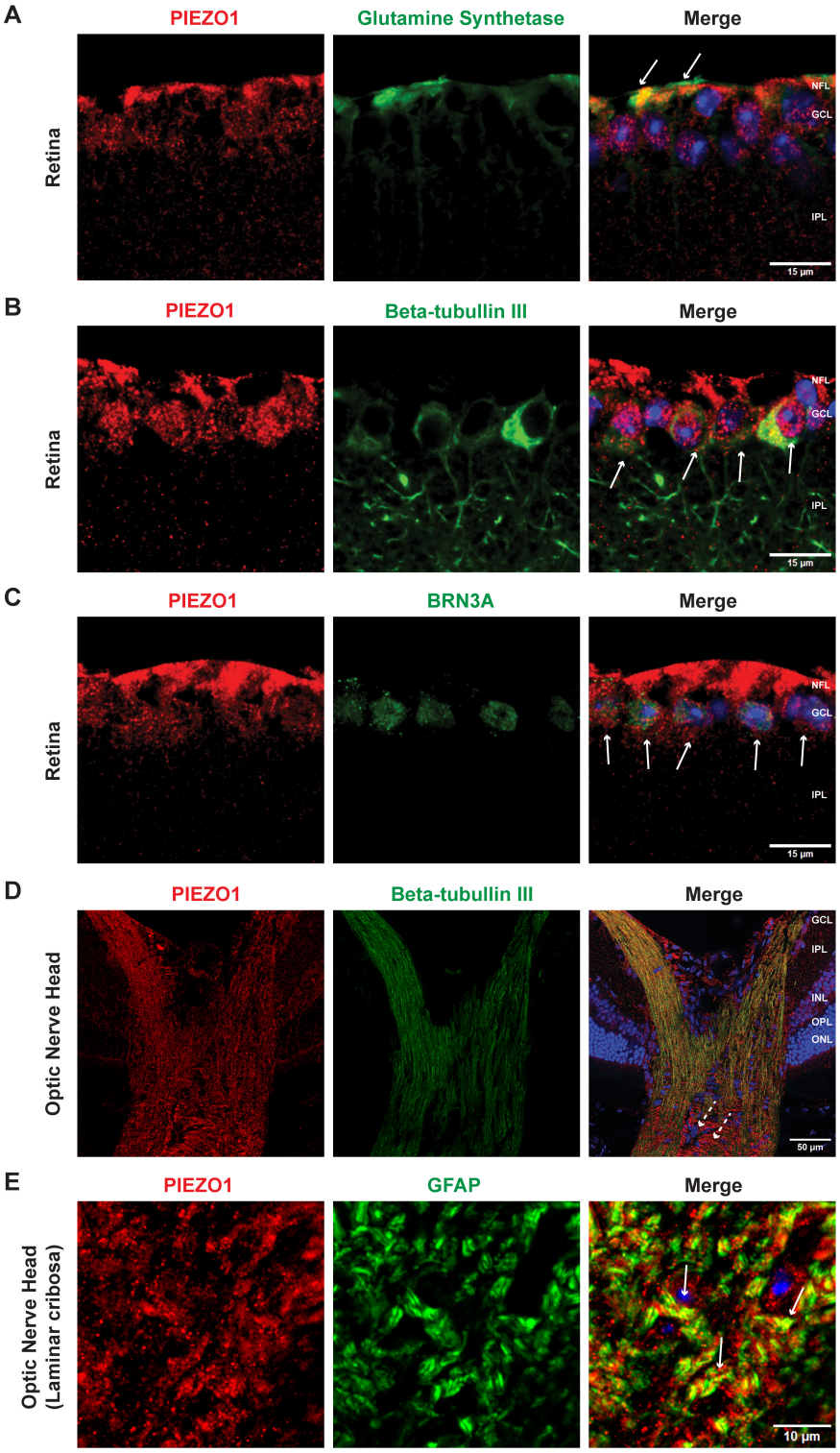

Figure 5.

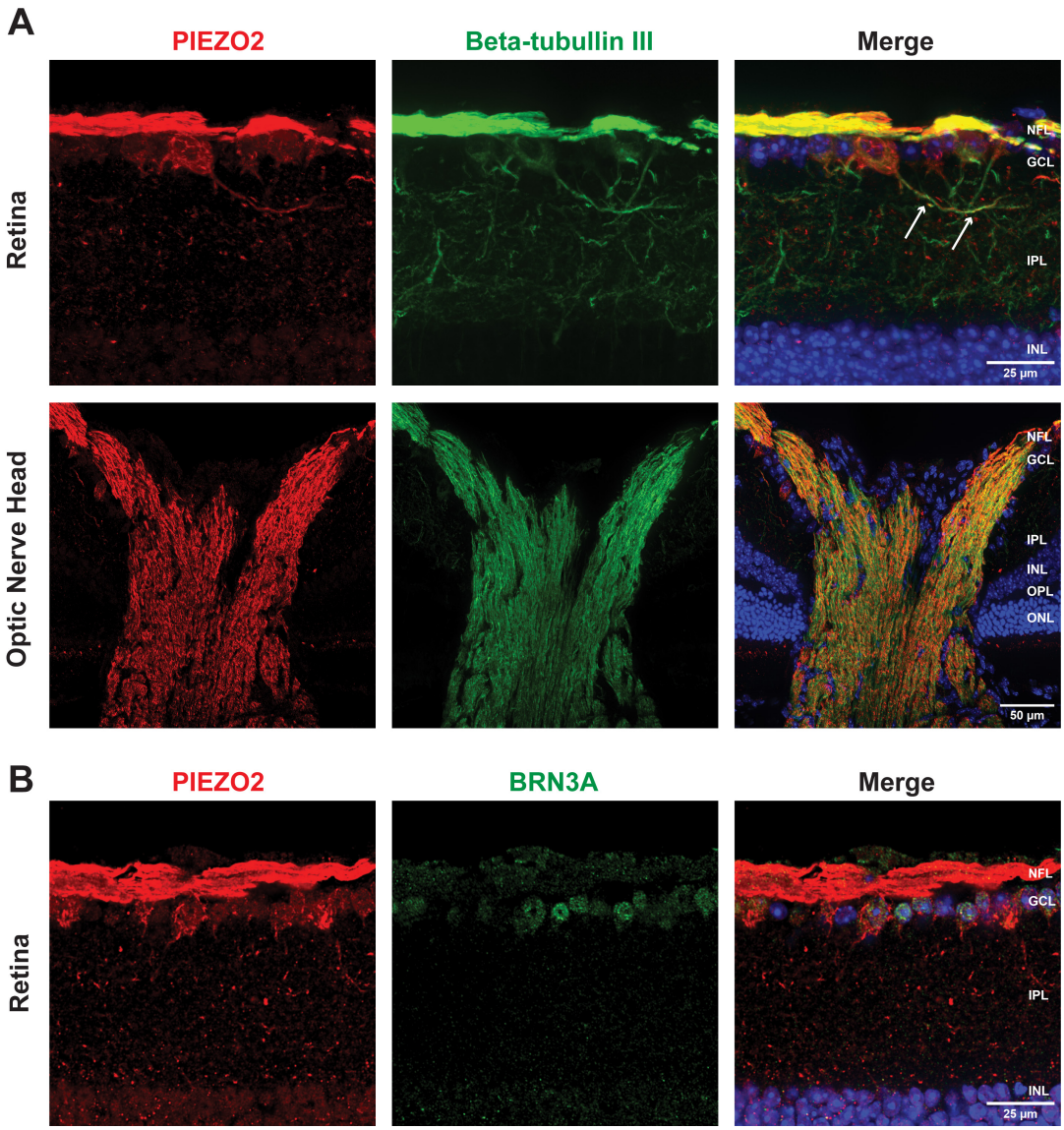

Figure 6.

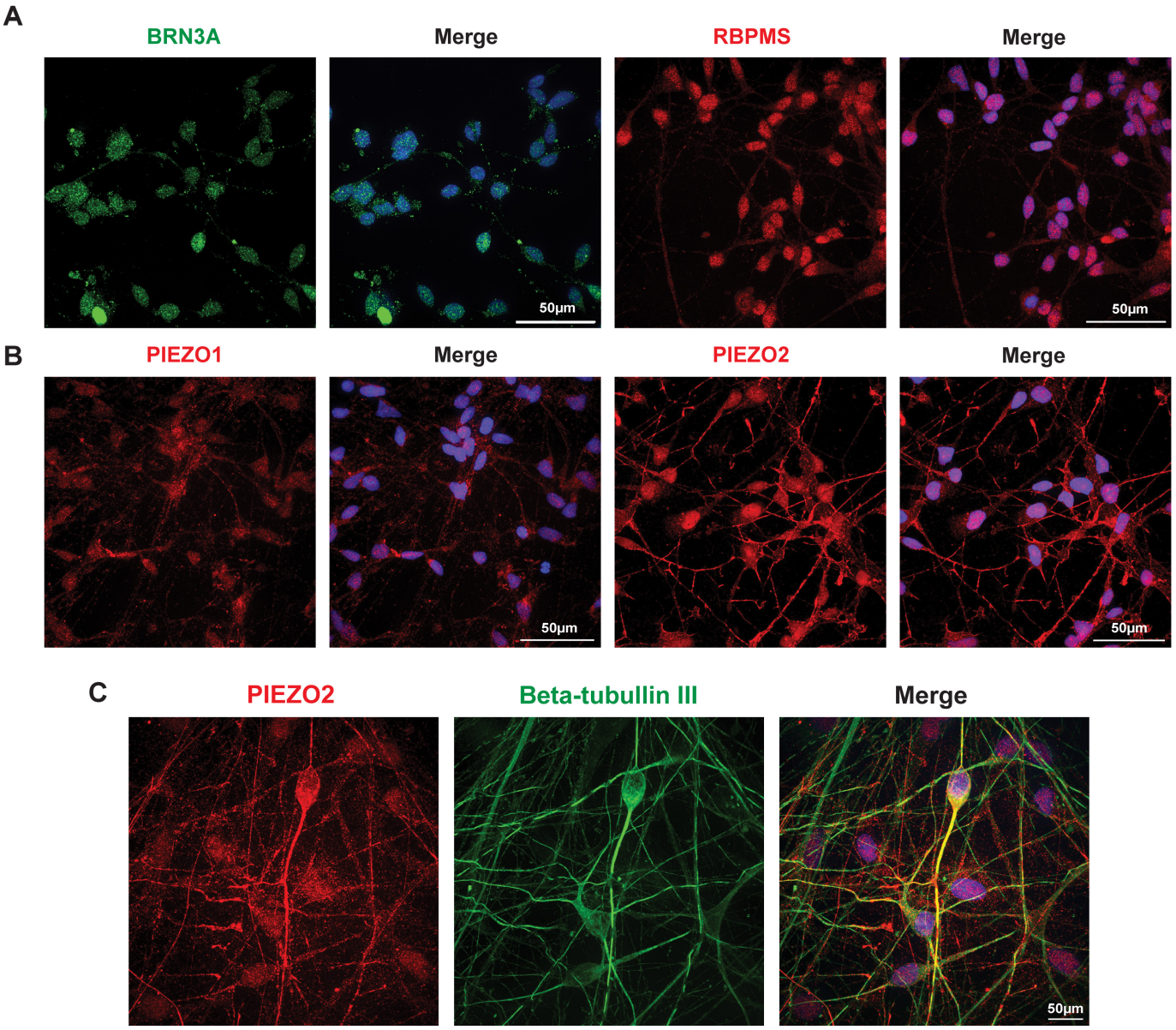

Figure 7.

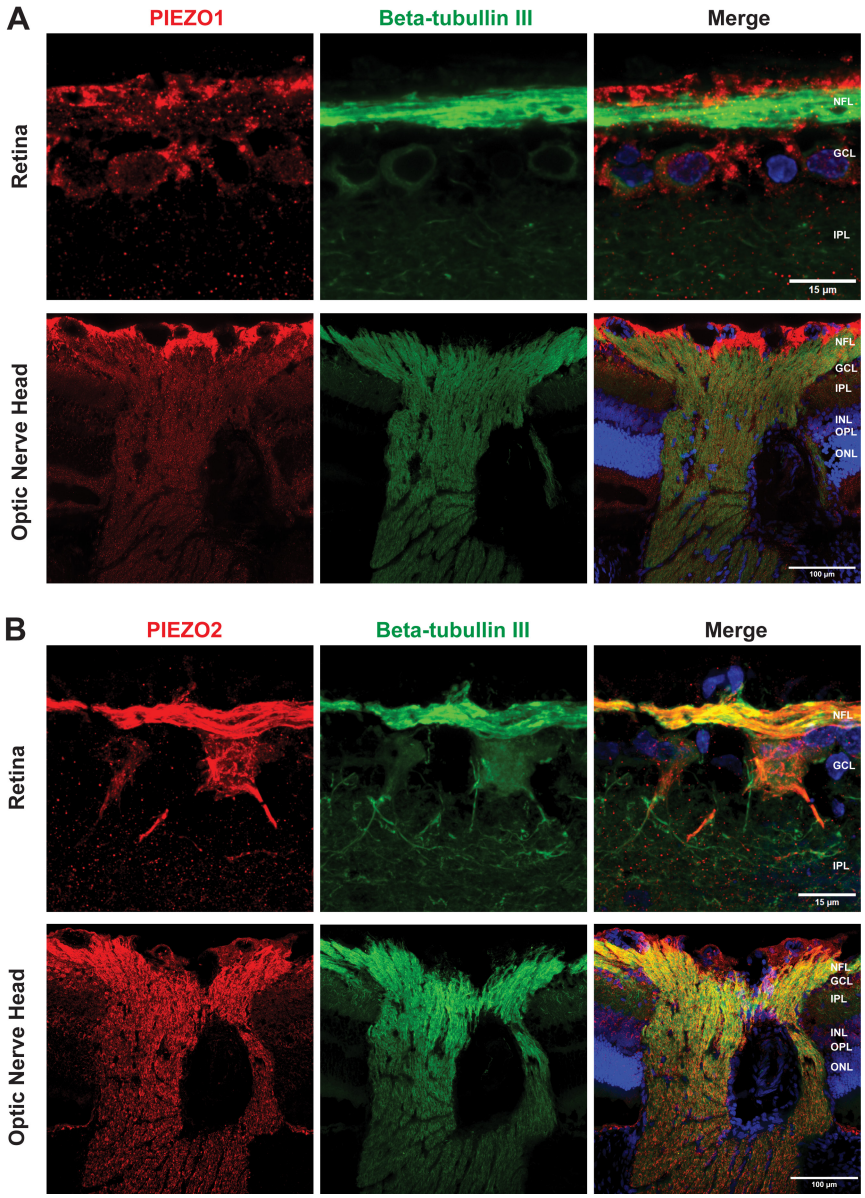

Table 1 List of primers

Gene name	Forward primer (5′–3′)	Reverse primer (3′–5′)	Size (bp)
Mouse Primers			
Piezo1	CCGTAGCCACATGATGCAG	TCACCCGAAGAAGCTCCTG	176
Piezo2	TGATTCATGCCTGTTGGTTG	TGAAATCCGGGAAGTACAGC	222
Gapdh	TCACCACCATGGAGAAGGC	GCTAAGCAGTTGGTGGTGCA	169
Human Primers			
PIEZO1	CAGGCCTATGAGGAGCTGTC	TTGTAGAGCTCCCGCTTCAT	170
PIEZO2	GCCCAACAAAGCCAGTTGAA	GGGCTGATGGTCCACAAAGA	167
GAPDH	GGTGTGAACCATGAGAAGTATGA	GAGTCCTTCCACGATACCAAAG	123

Table 2 List of antibodies

Antibody	Source	Identifier	Dilution
Primary Antibodies			
Rabbit anti-Piezo 1	Novus Biologicals	Cat# NBP1-78537, RRID:AB_11003149	1:100
Rabbit anti-Piezo 1	ProteinTech	Cat# 15939-1-AP, RRID:AB_2231460	1:100
Rabbit anti-Piezo 2	Novus Biologicals	Cat# NBP1-78624, RRID:AB_11005294	1:200
Biotin Mouse anti-Tubulin β3	Biolegend	Cat# 801212, RRID:AB_2721321	1:200
Mouse anti-Brn3a	Milipore	Cat# MAB1585, RRID:AB_94166	1:50
Goat anti-Brn3a	Santa Cruz Biotechnology	Cat# sc-31984, RRID:AB_2167511	1:200
Rabbit anti-RBPMS	GeneTex	Cat# GTX118619, RRID:AB_10720427	1:200
Goat anti-GFAP	Abcam	Cat# ab53554, RRID:AB_880202	1:200
Mouse anti-Glutamine synthetase	GeneTex	Cat# GTX630654, RRID:AB_2888230	1:200
Secondary Antibodies			
Donkey anti-Rabbit Alexa Fluor 647	Jackson Immunoresearch Labs	Cat# 711-605-152, RRID:AB_2492288	1:500
Donkey anti-Rabbit Alexa Fluor 568	Thermo Fisher Scientific	Cat# A-10042, RRID:AB_2534017	1:500
Alexa Fluor® 488 Streptavidin	Biolegend	Cat# 405235	1:500
Donkey anti-Goat Alexa Fluor 488	Thermo Fisher Scientific	Cat# A-21206, RRID:AB_2535792	1:500
Donkey anti-Mouse Alexa Fluor 488	Thermo Fisher Scientific	Cat# A-21202, RRID:AB_141607	1:500